Available online at www.sciencedirect.com
SCIENCE DIRECT®
Journal of Sound and Vibration 287 (2005) 245–276
JOURNAL OF SOUND AND VIBRATION
www.elsevier.com/locate/jsvi

Interactive power flow characteristics of an integrated equipment—nonlinear isolator—travelling flexible ship excited by sea waves

Y.P. Xiong[a,b,*], J.T. Xing[a], W.G. Price[a]

[a]*School of Engineering Sciences, Ship Science, University of Southampton, Southampton, SO17 1BJ, UK*
[b]*Institute of Engineering Mechanics, Shandong University, Jinan 250061, People's Republic of China.*

Received 3 December 2003; received in revised form 25 October 2004; accepted 2 November 2004
Available online 18 January 2005

Abstract

A nonlinear interactive system comprising of equipment, nonlinear isolator and travelling flexible ship excited by waves is studied from a vibratory power flow viewpoint to examine its dynamical behaviour and power flow characteristics. The mathematical model describing the dynamics of this nonlinear interactive system is developed. Dynamical interactions between equipment, nonlinear isolator, flexible foundation and water waves are addressed. The nonlinearities of the isolator are characterized by a general pth power model for damping and qth power for stiffness. A harmonic balance method is adopted to derive the steady-state harmonic response of the nonlinear system. A Newton–Raphson iteration process in association with an efficient numerical algorithm is used to obtain the solutions of this nonlinear problem. Through simulations the dynamical behaviour, power flow characteristics and isolation efficiency of this complex nonlinear interaction system are investigated. For different values of power p and q, different wave excitations and flexible or rigid ship, the power transmitted to the equipment and power flow transmission ratios are calculated and analysed. The effect of the vibration source with different wave conditions of the seaway is studied through examining its vibratory power input to the overall system. The effects of the assumptions of flexible or rigid ship, the nonlinearities on the power flows in the system are examined. Nonlinear power flow phenomena and mechanisms are revealed, which provides an insight to the

*Corresponding author. Tel.: +44 2380 596549; fax: +44 2380 193299.
E-mail addresses: y.p.xiong@ship.soton.ac.uk (Y.P. Xiong), j.t.xing@ship.soton.ac.uk (J.T. Xing), w.g.price@ship.soton.ac.uk (W.G. Price).

0022-460X/$ - see front matter
doi:10.1016/j.jsv.2004.11.009

understanding of power flow characteristics in nonlinear systems. Practical guidelines for the design of vibration isolation systems applicable to maritime engineering are suggested.

1. Introduction

Ships experience extreme motions when travelling in rough seas. These excite large forces on the hull and accelerations on equipment mounted in the vessels, and hence can significantly affect the operation quality and durability of the equipment and decrease overall safety. Therefore, it is important to protect equipment mounted on a ship operating in hostile environments. Vibration protection of sensitive equipment often relies on resilient mounts. Vibration isolators are used to reduce vibrations transmitted from a base to equipment (e.g. machinery, etc.) and they usually consist of passive and dissipative elements mounted between the equipment and foundation. The classical theory of vibration isolation [1–4] assumes the whole system is linear, the equipment and its supporting base are rigid and assumes a single degree-of-freedom (dof) system to model the isolator neglecting the dynamical interactions between the equipment, isolators and/or supporting structure. Based on this relatively simple model, a low suspension frequency ω_0 and lightly damped vibration isolator should provide efficient attenuation of harmonic vibration over a wide range of frequencies $\omega > \sqrt{2}\omega_0$. This type of model was studied by Tao et al. [5] in a problem relating to marine engineering, in which the isolation system was assumed linear and the marine engine was idealized as a rigid body with 6 dof supported by four isolators fixed to a rigid floor, but the investigation neglected any fluid–structure interactions from the seaway.

In reality, however, dynamical systems are inherently nonlinear and significant nonlinear behaviour has been observed in many vibration applications. For example, hydraulic engine mounts used in vehicles exhibit nonlinear stiffness and damping and their behaviour is sensitively dependent on excitation frequency and vibration amplitude [6,7]. Orifice type dampers produce nonlinear damping [8] and vibration isolators consisting of polymeric materials display nonlinear characteristics in both stiffness and damping [9]. In these isolation systems, the transmission path between source and receiver contains significant localized nonlinear elements. To design a practical isolation system with nonlinear elements, the current linear model cannot provide satisfactory performance. Moreover, the equipment and supporting structures are not rigid but in reality flexible and there exist dynamical interactions between the exciting source and receiving structures, which may lead to limitations in control capabilities. Such explanations provide reasons why unsatisfactory performance of vibration isolators can sometimes be observed in engineering applications. Therefore, to improve classical isolation design and to obtain better isolation performance, two areas of investigation are required. One is the linear dynamic characteristic of the source, receiver, isolators and their interactions, and the other is nonlinearity.

The investigation of the effect of flexible equipment or supporting structure on isolation system design using a linear model usually involves the examination of isolation performance in terms of force or motion transmissibility [10–13]. Based on these fundamental studies, it was shown [14–20] that compliant equipment, wave effects experienced by the isolator and the dynamical behaviour of the supporting structure can significantly affect the system's performance and the mobility of

the base structure plays an important role in the overall behaviour of the isolation system. A recent investigation [21] of the dynamics and control of the human body—passive/active seat suspension—vessel—wave system has revealed that the interactive effect between the elastic vessel and a human body-seat suspension system is significant. Hence, the dynamical behaviour of the ship should be considered in a conventional seat design for lightly damped high-speed vessels.

Recently, investigators [5–8,22–24] have re-examined the classical linear theory of vibration isolation and shown that inclusion of nonlinearity present in practical isolators becomes very important. In 1995, Kim and Singh [7] studied nonlinear dynamic characteristics of a hydraulic engine mount both at the device level and within the context of a simplified 2 dof vehicle model constructed by a nonlinear mount and a linear suspension system. The effects of nonlinear orifice type damping on the response of 1 and 2 dof systems were reported by Popov and Sankar [8]. Ravindra and Mallik [22] investigated the dependence of transmissibility performance on the nonlinear parameters of isolators in a 1 dof configuration. The performance of nonlinear isolators, subject to shock excitations, with four different damping characteristics was examined by Shekhar et al. [23]. Natsiavas and Tratskas [24] investigated a 2 dof system consisting of a rigid body on two identical isolators characterized by linear viscous damping and Duffing-type stiffness. In these studies, although the nonlinearity existing in local components was considered, however, the dynamical coupling effects of source and/or receiving structure were neglected due to the assumption of rigidity for equipment and supporting structures.

Vibratory power flow provides a performance descriptor accounting for both force and motion characteristics [14,15], which can describe more accurately the dynamical behaviour of vibration systems. In recent years, a power flow analysis (PFA) method has been successfully developed to model linear complex structures/structural-acoustic and vibration control systems [14–20,25–31]. Many investigators have developed various methods [14–20] to predict power flow transmissions in linear dynamical systems. The power flow parameter is also chosen as a cost function to evaluate the performance of optimal vibration control [25–31]. It is surprising that investigations into power flow analysis of nonlinear systems are very limited although Royston and Singh [32,33] studied nonlinear vibration isolation systems using a vibratory power transmission approach.

To address the described problems, Xiong et al. [34] studied a nonlinear isolation system comprising of a nonlinear damper and spring supporting equipment in a floating flexible ship using a power flow approach. An integrated mathematical model was developed to include nonlinearity effects and interactions between equipment, isolator and flexible structure. However, to simplify the problem, the ship was assumed stationary and therefore wave effects were neglected. That is, the coupling effects between waves and the dynamical behaviour of the ship on power transmission characteristics were not addressed. In numerical simulations, only nonlinear characteristics of typical quadratic damping and/or stiffness were examined.

In contrast to normal vibration isolation systems usually involving large solid foundation structures fixed to the earth, the isolation systems used in ships travelling in a seaway must handle distinct features such as wave–structure interactions. For example, a ship is a large elastic structure travelling in a seaway experiencing wave loads of differing frequency content. These wave loads are distributed dynamic forces acting on the wetted surface of the ship and therefore there exists a strong coupling with the displacement of the flexible structure. The generalized forces exciting the motions of equipment are strongly dependent on both wave parameters and structural dynamic behaviour. Furthermore, the whole floating system may experience a large

motion and/or large impact forces produced by slams or impacts whilst travelling in rough seas. As a result of these, the isolation system may often experience a large transient displacement, and therefore the nonlinearity in springs and dampers in the suspension system used in floating structures cannot be ignored. Due to these aspects of marine engineering, it is a challenging problem to investigate an integrated dynamical system including the interactive behaviour of the whole coupling system as well as the nonlinear characteristics of isolators used in high-speed vessels travelling in seaways.

In this paper, a mathematical model and power flow analysis theory [34] are further developed to describe the dynamical behaviour of a coupled system involving nonlinear isolation systems supporting equipment in a flexible ship travelling at a constant speed in a seaway. The ship is excited by distributed dynamic loadings produced by sinusoidal sea waves of unit wave amplitude and a selection of wavelengths $\lambda = 0.105L$, $0.349L$, $2L$, L, $L/2$, $L/4$. The nonlinear dynamical characteristics of the isolator are described by a general nonlinear model consisting of a pth power damper and a qth power stiffness. Not only are both stiffness and damping nonlinearities considered, but also the beamlike ship is treated as flexible and the vibration source effect due to the coupling of the sinusoidal waves and hull included. That is, the hull is subject to fluid actions involving inertial, damping and buoyancy forces. The equations of motion describing the dynamical behaviour of the nonlinear interacting system are derived and a harmonic balance approach [35], in association with a Newton–Raphson iteration process [36], is adopted to derive the steady-state harmonic responses of the system.

To characterize and analyse the influence of nonlinear effects, nonlinear systems with several combinations of different damping and stiffness powers p and q are examined. Each nonlinear system is analysed using a power flow approach and calculations include instantaneous and time-averaged nonlinear power flow spectra. The influence of flexible or rigid ship, the effects of the nonlinearities in damping and/or in stiffness, and the impact of different wave excitations on power flow characteristics are studied. The results of these nonlinear systems are compared with the linear case, i.e., $p = 1$ and $q = 1$ to illustrate power flow behaviour in the chosen nonlinear system.

2. Mathematical modelling

Fig. 1 illustrates schematically a dynamical interaction system comprising equipment (e.g. machinery), a nonlinear isolator and a flexible ship hull excited by waves. During operation, it is assumed that the high-speed vessel experiences severe hydrodynamic loading due to waves, slamming and wave impact phenomena. To predict the resultant motions of the vessel in a realistic manner, the mathematical model developed by Bishop et al. [37] contains many details of the ship (i.e., shape, mass distribution, etc.). However, in this study with its emphasis on nonlinear behaviour, to assess the interactions of the many components in the dynamical system (see for example, Fig. 1) and to understand the underlying mechanisms, a simple mathematical model [38,39] is assumed in which the ship is idealized as a uniform prismatic flexible beam of length L, breadth B, thickness h, draught d ($\leqslant h$), mass density per unit length ρ_b and bending stiffness EI. This uniform beam is symmetric port-starboard about the longitudinal x-axis and travels at constant speed U in a sinusoidal head wave of amplitude a, wavenumber k and absolute frequency

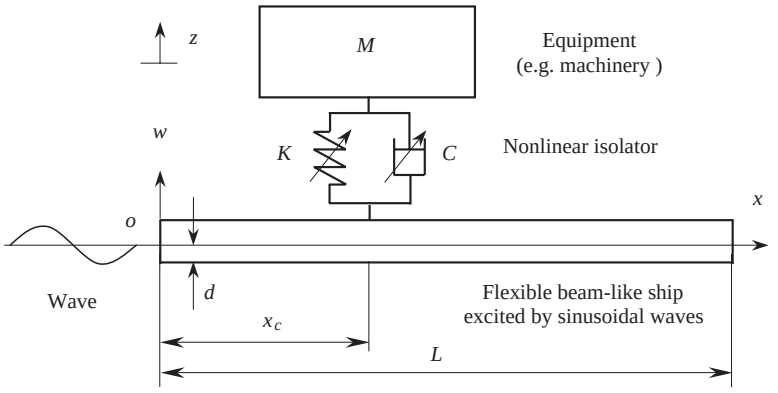

Fig. 1. Dynamic model of a nonlinear isolation system installed on a flexible beam subject to wave excitation.

ω. The ship experiences loadings from this wave system which is defined by the profile $\xi(x,t) = a\sin(kx-\omega_e t)$ where the frequency of wave encounter between ship and wave is $\omega_e = \omega - U\omega^2/g$ [39].

The governing equations describing the nonlinear interactive system are as follows:

$$M\ddot{\delta} + f_c(\delta,\dot{\delta}) = -M\ddot{w}(x_c,t), \tag{1a}$$

$$\delta(t) = z(t) - w(x_c,t), \tag{1b}$$

$$f_c(\delta,\dot{\delta}) = C\dot{\delta}|\dot{\delta}|^{p-1} + K\delta|\delta|^{q-1}, \tag{1c}$$

$$EI\frac{\partial^4 w}{\partial x^4} + \rho_b\frac{\partial^2 w}{\partial t^2} = f(\xi,w,x,t) + f_c D(x-x_c), \tag{2a}$$

$$f(\xi,w,x,t) = \rho_a\left(\frac{\partial^2\xi}{\partial t^2} - \frac{\partial^2 w}{\partial t^2}\right) + b\left(\frac{\partial\xi}{\partial t} - \frac{\partial w}{\partial t}\right) + k_w(\xi - w), \tag{2b}$$

$$\xi(x,t) = a\ \sin(kx-\omega_e t), \quad \omega_e = \omega - U\omega^2/g, \tag{2c}$$

$$\left.\frac{\partial^2 w}{\partial x^2}\right|_{x=0} = 0 = \left.\frac{\partial^2 w}{\partial x^2}\right|_{x=L}, \quad \left.\frac{\partial^3 w}{\partial x^3}\right|_{x=0} = 0 = \left.\frac{\partial^3 w}{\partial x^3}\right|_{x=L}, \tag{3}$$

where D denotes a delta function, M the mass of the equipment under investigation, z and $w(x_c,t)$ are the absolute displacements of the mass and beam at the point x_c, respectively. $f_c(\delta,\dot{\delta})$ represents the restoring force of the nonlinear isolator in which C and K are the damping and stiffness coefficients, respectively. Eq. (2a) describes both a travelling and stationary beam vibrating in water, because the encounter frequency is dependent on the forward speed U of the beam-like ship. If $U=0$, then $\omega_e = \omega$, which represents the case of a stationary beam. The exponents p and q in Eq. (1c) characterize, respectively, the nature of the nonlinearity in damping and stiffness of the isolator. This model can be considered as an idealization of a variable diaphragm pneumatic suspension system [40]. With $q=3$, we obtain a generalized Duffing

equation model with pth power damping [22]. With $q = 1$ and $p = 1$, Eq. (1) reduces to the linear case.

In Eq. (2b), $f(\xi, w, x, t)$ denotes the fluid loading per unit length involving inertial, damping and buoyancy forces, which is assumed to be a function of the relative motion $\xi - w$ between sinusoidal wave and the vertical displacement of the beam and can be rewritten as

$$f(\xi, w, x, t) = f_{\xi} - f_{w}, \tag{4}$$

where $f_{\xi} = f_{(\xi)}$, $f_{w} = f_{(w)}$, in which $f_{(\,)} = \rho_a \partial^2(\,)/\partial t^2 + b\partial(\,)/\partial t + k_w(\,)$. The substitution of wave equation (2c) into (4) yields

$$f_{\xi} = a(k_w - \rho_a \omega_e^2)\sin(kx - \omega_e t) - ab\omega_e^2 \cos(kx - \omega_e t), \tag{5}$$

where $k_w = \rho g B$ denotes buoyancy stiffness and ρ the density of the sea. The constants ρ_a and b are referred to as the added mass and fluid damping of the floating beam, respectively [39]. Physically, in the mathematical model accepted in this study, the rudimentary specification of the fluid actions relates to the relative displacement, relative velocity and relative acceleration between the wave elevation and the vertical response of the flexible beam-like hull, as indicated in Eq. (2b). These assumed constants imply averaged parameter values over the frequency range of interest to provide a first approximation to the problem. In a more realistic hydroelastic mathematical model [37,39], these parameters depend on the geometrical hull shape, forward speed, heading angle between ship and waves, frequency of encounter and environmental conditions. Such model complexities magnify numerical procedures with refinement of solution accuracy without significantly altering concepts or qualitative findings.

The introduction of these simplifications to the theory does not affect the generality of the mathematical model described herein because the natural modes of the dry hull are used in the mode summation method [37,39] adopted to solve the complex interactive dynamic system. The simplified model may be replaced by more sophisticated mathematical models, the sinusoidal wave replaced by a profile of an irregular seaway, convolution integrals adopted to describe the fluid actions, etc., but fundamental modal solutions based on the dry free–free hull treated in vacuo remain unchanged.

3. Solution procedure and dynamical analysis

3.1. Natural mode functions of the dry free–free beam and its orthogonal relations

Here, the natural vibration of a linear uniform dry free–free beam is examined, which is governed by the following equations:

$$EI\,\frac{\partial^4 w}{\partial x^4} + \rho_b\,\frac{\partial^2 w}{\partial t^2} = 0, \tag{6a}$$

$$\frac{\partial^2 w}{\partial x^2} = 0, \quad \frac{\partial^3 w}{\partial x^3} = 0, \quad x = 0, \tag{6b}$$

$$\frac{\partial^2 w}{\partial x^2} = 0, \quad \frac{\partial^3 w}{\partial x^3} = 0, \quad x = L. \tag{6c}$$

By solving the characteristic equations of the system, see, for example Refs. [3,4], the natural frequencies and the corresponding mode functions are obtained as follows:

Natural frequencies:

$$\tilde{\omega}_0 = 0 = \tilde{\omega}_1, \quad \tilde{\omega}_n^2 = \frac{EI}{\rho_b}\,\beta_n^4 \quad (n = 2, 3\ldots), \tag{7a}$$

Natural modes:

$$W_0(x) = 1, \quad W_1(x) = 2x/L - 1,$$

$$W_n(x) = \cosh\,\beta_n x + \cos\,\beta_n x + \alpha_n(\sinh\,\beta_n x - \sin\,\beta_n x), \quad (n = 2, 3, \ldots), \tag{7b}$$

$$\alpha_n = -\frac{\cosh\,\beta_n L - \cos\,\beta_n L}{\sinh\,\beta_n L + \sin\,\beta_n L} \quad (n = 2, 3, \ldots), \tag{7c}$$

where $W_0(x)$ and $W_1(x)$ are the heave and pitch rigid body modes of the beam, respectively, with relevant natural frequencies $\tilde{\omega}_0 = 0 = \tilde{\omega}_1$. These natural modes satisfy orthogonal relations [3,4],

$$\int_0^L W_i(x)W_j(x)\,\mathrm{d}x = m_I\delta_{ij}, \quad \int_0^L W_i''(x)W_j''(x)\,\mathrm{d}x = k_I\delta_{ij} \quad (i,j = 0, 1, 2, 3, \ldots, I = i), \tag{7d,e}$$

where $(\,)'' = \partial^2(\,)/\partial x^2$, m_I and k_I are the corresponding values of the integrations and δ_{ij} represents the Kronecker delta. These natural mode functions $W_i(x)$, $(i = 0, 1, 2, 3\ldots)$ form a series of complete and orthogonal functions defined in the domain $(x \in (0, L))$. Obviously, these functions are continuous and sufficiently differentiable within the defined domain and independent of any external forces. Therefore, any sufficiently differentiable function w(x), such as the displacement of the beam caused by any forces, can be represented by the following series:

$$w(x) = \sum_{n=0}^{\infty} W_i(x)\varsigma_i, \quad \varsigma_i = \int_0^L W_i(x)w(x)\,\mathrm{d}x/m_I, \tag{7f,g}$$

because there exist the integrations represented by Eq. (7g) to provide the coefficients ς_i.

3.2. Mode representation of the beam displacement response

The dynamic displacement w (x, t) of the beam satisfying Eq. (2a) is a single-value, continuous and differentiable function of x defined in the domain $x \in (0, L)$, because the beam is assumed to have no discontinuity or multi-values of the displacement at any point $x \in (0, L)$ during its motion. Therefore, based on the descriptions in Section 3.1, the dynamic displacement w (x, t) of the beam can be represented using an arbitrary series of complete functions defined in the domain $x \in (0, L)$. Here the series of the mode functions $W_i(x)$of the dry beam are chosen [39,41] and the dynamic displacement w (x, t) is represented as

$$w(x, t) = \sum_{n=0}^{N} W_n(x)q_n(t), \tag{8}$$

where $q_n(t)(n = 0,1,2\ldots)$ denotes a time-dependent generalized coordinates, and N denotes the maximum mode number adopted in the analysis to achieve a prescribed accuracy of solution.

Substituting Eq. (2b) into Eq. (2a) yields

$$EI\frac{\partial^4 w}{\partial x^4} + (\rho_a + \rho_b)\frac{\partial^2 w}{\partial t^2} + b\frac{\partial w}{\partial t} + k_w w = \rho_a \frac{\partial^2 \xi}{\partial t^2} + b\frac{\partial \xi}{\partial t} + k_w \xi + f_c D(x - x_c). \tag{9a}$$

Substituting Eq. (8) into Eq. (9a), then pre-multiplying $W_i(x)$ on both sides and integrating with respect to x from 0 to L using the orthogonal relations Eqs. (7d,e) and noting the delta function $D(x - x_c)$in the integration, we obtain

$$\ddot{q}_n + 2\xi_n \omega_n \dot{q}_n + \omega_n^2 q_n = Q_n(t)/M_n + f_c(\delta, \dot{\delta}) W_n(x_c)/M_n \quad (n = 0, 1, 2, \ldots, N). \tag{9b}$$

Here $\omega_n = \sqrt{K_n/M_n}$, $\xi_n = C_n/2M_n\omega_n$, M_n, C_n, K_n and $Q_n(t)$ are generalized mass, damping, stiffness and force represented, respectively, by the forms

$$M_n = \int_0^L (\rho_a + \rho_b) W_n^2(x)\,\mathrm{d}x,$$

$$C_n = \int_0^L b W_n^2(x)\,\mathrm{d}x,$$

$$K_n = \int_0^L [EI\, W_n''^2(x) + k_w W_n^2(x)]\,\mathrm{d}x,$$

$$Q_n(t) = \int_0^L f_\xi W_n(x)\,\mathrm{d}x, \quad f_\xi = \rho_a \frac{\partial^2 \xi}{\partial t^2} + b\frac{\partial \xi}{\partial t} + k_w \xi. \tag{9c}$$

Eq. (9b) is a set of differential equations with $N+2$ unknown variables $q_n(t)$, $(n = 0, 1, 2, \ldots, N)$ and $\delta(t)$ to be determined by solving Eq. (9b) and Eq. (1a).

3.3. Nondimensional form of equations

By choosing the characteristic length of the wave amplitude a, time $1/\Omega_0$, $\left(\Omega_0 = \sqrt{Ka^{q-1}/M}\right)$, and mass M, the nonlinear Eqs. (1a) and (9b) can be rewritten in their nondimensional forms,

$$\ddot{\Delta} + \bar{f}_c(\Delta, \dot{\Delta}) = -\ddot{\bar{w}}(\bar{x}_c, T), \tag{10a}$$

$$\ddot{\bar{q}}_n + 2\xi_n \Xi_n \dot{\bar{q}}_n + \Xi_n^2 \bar{q}_n = \bar{Q}_n \gamma_n + \bar{f}_c W_n(\bar{x}_c)\gamma_n \quad (n = 0, 1, 2, \ldots), \tag{10b}$$

$$\ddot{\bar{z}} + \bar{f}_c(\Delta, \dot{\Delta}) = 0, \tag{10c}$$

$$\bar{w} = \sum_{n=0}^{N} W_n(\bar{x})\bar{q}_n(T), \tag{10d}$$

where Eq. (1c) is expressed as

$$\bar{f}_c(\Delta, \dot{\Delta}) = 2\eta\dot{\Delta}|\dot{\Delta}|^{p-1} + \Delta|\Delta|^{q-1}. \tag{11}$$

Here Eq. (10c) is introduced to replace Eq. (1b) in order to calculate the absolute displacement $\bar{z}$ satisfying the dynamical equilibrium equation of the absolute motion of equipment using the harmonic balance method described in Section 3.4 and therefore, avoids numerical errors.

The corresponding nondimensional quantities in Eq. (10) are given as

$$\Delta = \frac{\delta}{a}, \quad \dot{\Delta} = \frac{\dot{\delta}}{a\Omega_0}, \quad \ddot{\Delta} = \frac{\ddot{\delta}}{a\Omega_0^2},$$

$$\bar{q}_n = \frac{q_n}{a}, \quad \dot{\bar{q}}_n = \frac{\dot{q}_n}{a\Omega_0}, \quad \ddot{\bar{q}}_n = \frac{\ddot{q}_n}{a\Omega_0^2},$$

$$\bar{w} = \frac{w}{a}, \quad \dot{\bar{w}} = \frac{\dot{w}}{a\Omega_0}, \quad \ddot{\bar{w}} = \frac{\ddot{w}}{a\Omega_0^2},$$

$$\bar{\xi} = \frac{\xi}{a}, \quad \bar{z} = \frac{z}{a}, \quad \bar{k} = ka,$$

$$\bar{b} = \frac{ab}{M\Omega_0}, \quad \bar{k}_w = \frac{ak_w}{M\Omega_0^2}, \quad \bar{Q}_n = \frac{Q_n}{Ma\Omega_0^2},$$

$$\gamma_n = \frac{M}{M_n}, \quad \gamma = \frac{M}{M_b},$$

$$\bar{\rho}_a = \frac{a\rho_a}{M}, \quad \bar{\rho}_b = \frac{a\rho_b}{M}, \quad \bar{\rho}_v = \bar{\rho}_a + \bar{\rho}_a,$$

$$\Xi_n = \frac{\omega_n}{\Omega_0}, \quad \Omega = \frac{\omega_e}{\Omega_0},$$

$$T = \Omega_0 t, \quad \omega_e t = \Omega T,$$

$$\eta = Ca^{p-1}\Omega_0^{p-2}/2M. \tag{12}$$

Accordingly, the generalized force is represented in terms of nondimensional parameters in the form

$$\bar{Q}_n = [\bar{S}_{1n} - \bar{b}\Omega\bar{S}_{2n}]\cos\ \Omega T - [\bar{S}_{2n} - \bar{b}\Omega\bar{S}_{4n}]\sin\ \Omega T, \tag{13a}$$

where

$$\bar{S}_{1n} = (\bar{k}_w - \bar{\rho}_a\Omega^2)\bar{S}_{4n}, \quad \bar{S}_{2n} = \int_0^{\bar{L}} W_n(\bar{x})\cos\ \bar{k}\bar{x}\,\mathrm{d}\bar{x},$$

$$\bar{S}_{3n} = (\bar{k}_w - \bar{\rho}_a\Omega^2)\bar{S}_{2n},$$

$$\bar{S}_{4n} = \int_0^{\bar{L}} W_n(\bar{x})\sin\bar{k}\bar{x}\,\mathrm{d}\bar{x} \quad (n = 0, 1, 2, \ldots, N). \tag{13b}$$

3.4. Harmonic balance method

The harmonic balance method [35] is a numerical tool applied in the frequency domain to study nonlinear dynamical problems. The general idea of this method is to represent each time history by its frequency content to obtain a set of equations by balancing the terms with the same frequency components and through an iterative procedure to find the roots of these equations. As a first approximation in the harmonic balance method, the dimensionless relative displacement Δ, the generalized coordinates $\bar{q}_n$, and the nonlinear coupling force $\bar{f}_c(\Delta, \dot{\Delta})$ are represented as Fourier expansions to the first order. Without loss of generality, we can arbitrarily choose $\Delta_0 = 0$ as a reference position in the Fourier expansion of the dimensionless relative displacement Δ. Therefore, we have

$$\Delta = \Delta_1 \cos(\Omega T + \phi), \tag{14}$$

$$\bar{q}_n = \bar{q}_{n0} + \bar{q}_{n1} \cos \Omega T + \bar{q}_{n2} \sin \Omega T \quad (n = 0, 1, 2, \ldots, N), \tag{15}$$

$$\begin{aligned} \bar{f}_c &= R_0 + R_1 \cos(\Omega T + \phi) + R_2 \sin(\Omega T + \phi) \\ &= R_0 + R \cos(\Omega T + \phi - \theta_{fc}), \end{aligned} \tag{16}$$

where ϕ is a phase angle, $\Delta_1, \bar{q}_{n0}, \bar{q}_{n1}$ and $\bar{q}_{n2}$ are coefficients of amplitudes to be determined. There is no necessity to include the phase ϕ in Eq. (16), but, as shown later in deriving Eqs. (54)–(57), it is a convenient parameter to use to derive the power flow absorption coefficient. R_0, R_1 and R_2 are the Fourier coefficients defined by

$$R_0 = \frac{1}{2\pi} \int_{-\pi}^{\pi} \bar{f}_c(\theta)\, \mathrm{d}\theta, \tag{17a}$$

$$R_1 = \frac{1}{\pi} \int_{-\pi}^{\pi} \bar{f}_c(\theta) \cos\theta\, \mathrm{d}\theta, \tag{17b}$$

$$R_2 = \frac{1}{\pi} \int_{-\pi}^{\pi} \bar{f}_c(\theta) \sin\theta\, \mathrm{d}\theta \tag{17c}$$

and

$$R(\Omega) = \sqrt{R_1^2 + R_2^2}, \quad \theta_{fc} = \tan^{-1} \frac{R_2}{R_1}, \tag{17d}$$

where $\theta = \Omega T + \phi$. Substituting Eq. (14) into Eqs. (11) and (17), and omitting the lengthy derivation of the integration, we find that the detailed expressions for R_0, R_1 and R_2 are given by

$$R_0 = 0, \quad R_1 = \lambda_q \Delta_1^q, \quad R_2 = -2\eta \Omega^p \lambda_p \Delta_1^p, \tag{18a–c}$$

where

$$\lambda_q = \frac{2}{\sqrt{\pi}} \frac{\Gamma(q/2 + 1)}{\Gamma(q/2 + 1.5)}, \quad \lambda_p = \frac{2}{\sqrt{\pi}} \frac{(p/2 + 1)}{\Gamma(p/2 + 1.5)},$$

in which Γ denotes the standard gamma function [42]. The substitution of Eqs. (14) and (16) into Eq. (10a) gives

$$-\Omega^2\Delta_1\cos(\Omega T+\phi)+R_1\cos(\Omega T+\phi)+R_2\sin(\Omega T+\phi)=-\sum_{n=0}^{N}W_n(\bar{x}_c)\ddot{\bar{q}}_n,$$

which when combined with Eqs. (15) and (18a) yield

$$(\lambda_q\Delta_1^q-\Omega^2\Delta_1)\cos\phi-2\eta\Omega^p\lambda_p\Delta_1^p\sin\phi=\Omega^2\sum_{n=0}^{N}\bar{q}_{n1}W_n(\bar{x}_c), \tag{19a}$$

$$(\lambda_q\Delta_1^q-\Omega^2\Delta_1)\sin\phi+2\eta\Omega^p\lambda_p\Delta_1^p\cos\phi=-\Omega^2\sum_{n=0}^{N}\bar{q}_{n2}W_n(\bar{x}_c). \tag{19b}$$

where coefficients of the same harmonics (i.e., $\sin\Omega T$, $\cos\Omega T$) and constant terms are equated. Similarly, from Eqs. (16), (10b) and (18a) it follows that

$$\bar{q}_{n0}=\frac{\gamma_n W_n(\bar{x}_c)}{\Xi_n^2}R_0=0, \tag{20a}$$

$$A_n^{(11)}\bar{q}_{n1}+A_n^{(12)}\bar{q}_{n2}-\alpha_n\Delta_1^q\cos\phi+\beta_n\Delta_1^p\sin\phi=F_{n1}, \tag{20b}$$

$$A_n^{(21)}\bar{q}_{n1}+A_n^{(22)}\bar{q}_{n2}+\alpha_n\Delta_1^q\sin\phi+\beta_n\Delta_1^p\cos\phi=F_{n2}, \tag{20c}$$

where

$$A_n^{(11)}=A_n^{(22)}=\Xi_n^2-\Omega^2,\quad A_n^{(12)}=-A_n^{(21)}=2\xi_n\Xi_n\Omega,$$

$$F_{n1}=\gamma_n[\bar{S}_{1n}-\bar{b}\Omega\bar{S}_{2n}],\quad F_{n2}=-\gamma_n[\bar{S}_{3n}-\bar{b}\Omega\bar{S}_{4n}],$$

$$\alpha_n=\gamma_n W_n(\bar{x}_c)\lambda_q,\quad \beta_n=2\eta\Omega^p\gamma_n W_n(\bar{x}_c)\lambda_p.$$

To solve the coupled nonlinear algebraic equations, we express Eqs. (19) and (20) in the matrix forms

$$\mathbf{A}_n\mathbf{Q}_n+\mathbf{B}_n\mathbf{X}=\mathbf{F}_n\quad(n=0,1,2,\ldots,N), \tag{21}$$

$$\sum_{n=0}^{N}W_n(\bar{x}_c)\mathbf{Q}_n+\mathbf{G}\mathbf{X}=\mathbf{0}\quad(n=0,1,2,\ldots,N), \tag{22}$$

where

$$\mathbf{A}_n=\begin{bmatrix}A_n^{(11)} & A_n^{(12)}\\ A_n^{(21)} & A_n^{(22)}\end{bmatrix}, \tag{23a}$$

$$\mathbf{B}_n=\begin{bmatrix}-\alpha_n\Delta_1^{q-1} & \beta_n\Delta_1^{p-1}\\ \beta_n\Delta_1^{p-1} & \alpha_n\Delta_1^{q-1}\end{bmatrix}, \tag{23b}$$

$$\mathbf{G} = \begin{bmatrix} 1 - \lambda_q \Delta_1^{q-1} \Omega^{-2} & 2\eta \Omega^{p-2} \lambda_p \Delta_1^{p-1} \\ 2\eta \Omega^{p-2} \lambda_p \Delta_1^{p-1} & -1 + \lambda_q \Delta_1^{q-1} \Omega^{-2} \end{bmatrix}, \tag{23c}$$

$$\mathbf{Q}_n = \begin{Bmatrix} \bar{q}_{n1} \\ \bar{q}_{n2} \end{Bmatrix}, \quad \mathbf{F}_n = \begin{Bmatrix} F_{n1} \\ F_{n2} \end{Bmatrix}, \tag{23d,e}$$

$$\mathbf{X} = \begin{Bmatrix} X_1 \\ X_2 \end{Bmatrix} = \begin{Bmatrix} \Delta_1 \cos\phi \\ \Delta_1 \sin\phi \end{Bmatrix}, \quad \mathbf{X}^{\mathrm{T}}\mathbf{X} = \Delta_1^2, \quad \phi = \tan^{-1}\frac{X_2}{X_1} \tag{23f}$$

To aid calculation, Eqs. (23b) and (23c) are written as

$$\mathbf{B}_n = \alpha_n \Delta_1^{q-1} \mathbf{I}_1 + \beta_n \Delta_1^{p-1} \mathbf{I}_2, \tag{24a}$$

$$\mathbf{G} = -\mathbf{I}_1 + \lambda_q \Delta_1^{q-1} \Omega^{-2} \mathbf{I}_1 + 2\eta \Omega^{p-2} \lambda_p \Delta_1^{p-1} \mathbf{I}_2, \tag{24b}$$

where the matrices $\mathbf{I}_1$ and $\mathbf{I}_2$ are given by

$$\mathbf{I}_1 = \begin{bmatrix} -1 & 0 \\ 0 & 1 \end{bmatrix}, \quad \mathbf{I}_2 = \begin{bmatrix} 0 & 1 \\ 1 & 0 \end{bmatrix}. \tag{24c,d}$$

The set of equations (21) and (22) is of nonlinear form and no exact general solution exists. However, many numerical methods can be used to solve such nonlinear system problems, e.g. a Newton–Raphson iteration process [36]. In the present study, this method is again adopted to solve the resulting nonlinear equations and the developed iterative algorithm (with good convergence characteristics) is presented in the following section. Obviously, if $p = 1$ and $q = 1$, the matrices $\mathbf{B}_n$ and $\mathbf{G}$ are independent of Δ_1 and the system equation (22) reduces to a linear form. The responses of this linear system can be determined by linear algebraic calculations following traditional procedures [43].

4. Iteration algorithm

To solve the coupled nonlinear Eqs. (21) and (22), we combine these two equations. That is

$$\mathbf{f}(\Delta_1, \Omega)\mathbf{X}(\Delta_1) = \mathbf{F}(\Omega), \tag{25}$$

where

$$\mathbf{f}(\Delta_1, \Omega) = \sum_{n=0}^{N} W_n(\bar{x}_c)\mathbf{A}_n^{-1}\mathbf{B}_n - \mathbf{G}, \tag{26a}$$

$$\mathbf{F}(\Omega) = \sum_{n=0}^{N} W_n(\bar{x}_c)\mathbf{A}_n^{-1}\mathbf{F}_n \tag{26b}$$

Eq. (25) is a nonlinear vector equation where the vector $\mathbf{f}(\Delta_1, \Omega)$ depends nonlinearly on the displacement Δ_1 and requires solving iteratively. The solution $\mathbf{X}$ at each excitation frequency Ω is determined using the Newton–Raphson iteration method.

The basic equation to be solved in this nonlinear analysis is described by Eq. (25) and at frequency $\Omega + \Delta\Omega$, we have

$$\mathbf{f}(\Delta_1, \Omega + \Delta\Omega)\mathbf{X}(\Delta_1(\Omega + \Delta\Omega)) = \mathbf{F}(\Omega + \Delta\Omega). \tag{27}$$

At each iterative step, the coefficients are evaluated at each exciting frequency.

Suppose the exact solutions at frequency Ω are X^* and Δ_1^*. They, therefore, satisfy Eq. (25), such that

$$\mathbf{f}(\Delta_1^*)\mathbf{X}^* = \mathbf{F}^*. \tag{28}$$

We assume that in the iterative solution the evaluated approximate values for Eq. (25) at frequency $\Omega + \Delta\Omega$ are $\Delta_1^{(i-1)}(\Omega + \Delta\Omega)$ and $\mathbf{X}^{(i-1)}(\Omega + \Delta\Omega)$. A Taylor series expansion of the first order gives the iterative solution $\mathbf{X}^{(i-1)}$ at the $(i-1)$th iteration which satisfies the relation

$$\begin{aligned}\mathbf{f}(\Delta_1^*)\mathbf{X}^* = \mathbf{f}(\Delta_1^{(i-1)}\Omega + \Delta\Omega)\mathbf{X}^{(i-1)}(\Omega + \Delta\Omega) + \left(\frac{\partial \mathbf{f}}{\partial \Delta_1}\mathbf{X}\right)\Bigg|_{\Omega+\Delta\Omega}^{(i-1)}[\Delta_1^* - \Delta_1^{(i-1)}(\Omega + \Delta\Omega)] \\ + \mathbf{f}|_{\Omega+\Delta\Omega}^{(i-1)}[\mathbf{X}^* - \mathbf{X}^{(i-1)}(\Omega + \Delta\Omega)],\end{aligned} \tag{29}$$

where higher-order terms are neglected. Substituting Eq. (28) into Eq. (29) and rearranging, we obtain

$$\begin{aligned}\left(\frac{\partial \mathbf{f}}{\partial \Delta_1}\mathbf{X}\right)\Bigg|_{\Omega+\Delta\Omega}^{(i-1)}[\Delta_1^* - \Delta_1^{(i-1)}(\Omega + \Delta\Omega)] + \mathbf{f}\Big|_{\Omega+\Delta\Omega}^{(i-1)}[\mathbf{X}^* - \mathbf{X}^{(i-1)}(\Omega + \Delta\Omega)] \\ = \mathbf{F}^* - \mathbf{f}(\Delta_1^{(i-1)}, \Omega + \Delta\Omega)\mathbf{X}^{(i-1)}(\Omega + \Delta\Omega).\end{aligned} \tag{30}$$

The substitution of the incremental corrections $\tilde{\Delta}_1 = \Delta_1^* - \Delta_1^{(i-1)}(\Omega + \Delta\Omega)$ and $\Delta\mathbf{X}^{(i)} = \mathbf{X}^* - \mathbf{X}^{(i-1)}(\Omega + \Delta\Omega)$, allows Eq. (30) to be written in the form

$$\left(\frac{\partial \mathbf{f}}{\partial \Delta_1}\mathbf{X}\right)\Bigg|_{\Omega+\Delta\Omega}^{(i-1)}\tilde{\Delta}_1 + \mathbf{f}|_{\Omega+\Delta\Omega}^{(i-1)}\Delta\mathbf{X}^{(i)} = \mathbf{F}^* - \mathbf{f}\mathbf{X}|_{\Omega+\Delta\Omega}^{(i-1)}. \tag{31}$$

Recognizing that $\mathbf{X}^{\mathrm{T}}\mathbf{X} = \Delta_1^2$, after differentiation we obtain

$$\tilde{\Delta}_1^{(i)} = \frac{1}{\Delta_1}\mathbf{X}^{\mathrm{T}}\Big|_{\Omega+\Delta\Omega}^{(i-1)}\Delta\mathbf{X}^{(i)}. \tag{32}$$

The substitution of Eq. (32) into Eq. (31) and using Eq. (27) yields

$$\left[\frac{1}{\Delta_1}\left(\frac{\partial \mathbf{f}}{\partial \Delta_1}\mathbf{X}\mathbf{X}^{\mathrm{T}}\right) + \mathbf{f}\right]\Bigg|_{\Omega+\Delta\Omega}^{(i-1)}\Delta\mathbf{X}^{(i)} = \mathbf{F}(\Omega + \Delta\Omega) - \mathbf{f}\mathbf{X}|_{\Omega+\Delta\Omega}^{(i-1)}. \tag{33}$$

The partial differentiation $\partial\mathbf{f}/\partial\Delta_1$ in this equation can be derived from Eqs. (24) and (26a) and is given by

$$\frac{\partial \mathbf{f}}{\partial \Delta_1} = \sum_{n=0}^{\infty} W_n(\bar{x}_c)\mathbf{A}_n^{-1}\frac{\partial \mathbf{B}_n}{\partial \Delta_1} - \frac{\partial \mathbf{G}}{\partial \Delta_1}, \tag{34}$$

$$\frac{\partial \mathbf{B}_n}{\partial \Delta_1} = \begin{bmatrix} -\alpha_n(q-1)\Delta_1^{q-2} & \beta_n(p-1)\Delta_1^{p-2} \\ \beta_n(p-1)\Delta_1^{p-2} & \alpha_n(q-1)\Delta_1^{q-2} \end{bmatrix}$$
$$= (q-1)\alpha_n\Delta_1^{q-2}\mathbf{I}_1 + (p-1)\beta_n\Delta_1^{p-2}\mathbf{I}_2, \quad (n = 0, 1, 2, \ldots, N), \tag{35}$$

$$\frac{\partial \mathbf{G}}{\partial \Delta_1} = \begin{bmatrix} -\lambda_q(q-1)\Delta_1^{q-2}\bar{\Omega}^{-2} & 2\eta(p-1)\bar{\Omega}^{p-2}\lambda_p\Delta_1^{p-2} \\ 2\eta(p-1)\bar{\Omega}^{p-2}\lambda_p\Delta_1^{p-2} & \lambda_q(q-1)\Delta_1^{q-2}\bar{\Omega}^{-2} \end{bmatrix}$$
$$= (q-1)\lambda_q\Delta_1^{q-2}\Omega^{-2}\mathbf{I}_1 + 2(p-1)\eta\Omega^{p-2}\lambda_p\Delta_1^{p-2}\mathbf{I}_2. \tag{36}$$

Thus, we obtain the incremental correction $\Delta\mathbf{X}^{(i)}$ from Eq. (33), which is used to obtain the next displacement approximation

$$\mathbf{X}^{(i)}(\Omega + \Delta\Omega) = \mathbf{X}^{(i-1)}(\Omega + \Delta\Omega) + \Delta\mathbf{X}^{(i)}. \tag{37}$$

In addition, the incremental correction $\tilde{\Delta}_1^{(i)}$ is obtained from Eq. (32) using the result for $\Delta X^{(i)}$. That is, the displacement at iteration i is

$$\Delta_1^{(i)}(\Omega + \Delta\Omega) = \Delta_1^{(i-1)}(\Omega + \Delta\Omega) + \tilde{\Delta}_1^{(i)}. \tag{38}$$

The relationship between Eqs. (33), (37) and (38) constitute the Newton–Raphson iteration solution of Eq. (28) and the iteration is continued until convergence to a specified response accuracy is obtained. After evaluating solutions $\mathbf{X}^{(i)}$ and $\Delta_1^{(i)}$, the generalized coordinates $\bar{q}_{n1}$ and $\bar{q}_{n2}$ or $\mathbf{Q}_n^{(i)}$ are given by

$$\mathbf{Q}_n^{(i)} = \mathbf{A}_n^{-1}[\mathbf{F}_n - \mathbf{B}_n(\Delta_1^{(i)})\mathbf{X}^{(i)}] \quad (n = 0, 1, 2, \ldots,). \tag{39}$$

The initial conditions are determined by the parameter values

$$\Delta_1^{(0)} = 0, \quad \bar{q}_{n1}^{(0)} = \frac{\gamma_n\bar{k}_w}{\Xi_n^2}\bar{S}_{4n}, \quad \bar{q}_{n2}^{(0)} = \frac{\gamma_n\bar{k}_w}{\Xi_n^2}\bar{S}_{2n} \quad (n = 0, 1, 2, \ldots, N) \tag{40}$$

giving $X_1^{(0)} = 0 = X_2^{(0)}$.

5. Dynamical responses of the nonlinear system

The substitution of the iterative solution $\mathbf{X}$ described in Eq. (23f) into Eq. (39) leads to solutions of $\bar{q}_{n1}$ and $\bar{q}_{n2}$ in Eq. (15). When the solutions $\bar{q}_n(n = 0, 1, 2, \ldots, N)$ are substituted into Eqs. (10d), (10c), (16), (17d) and (18), the nondimensional absolute displacements $\bar{w}$ at position $\bar{x}$ of the beam and $\bar{z}$ at the centre of mass of the equipment are derived in the forms

$$w(\bar{x}, \Omega, T) = \Delta_w(\bar{x}, \Omega)\cos(\Omega T - \theta_w), \tag{41}$$

$$\bar{z}(T, \Omega) = \Delta_z(\Omega)\cos(\Omega T + \theta_z), \tag{42}$$

where

$$\Delta_w(\bar{x},\Omega)=\sqrt{\left[\sum_{n=0}^{N}W_n(\bar{x})\bar{q}_{n1}\right]^2+\left[\sum_{n=0}^{N}W_n(\bar{x})\bar{q}_{n2}\right]^2}, \tag{43a}$$

$$\Delta_{wc}(\Omega)=\Delta_w(\bar{x}_c,\Omega), \tag{43b}$$

$$\Delta_z(\Omega)=R(\Omega)/\Omega^2, \tag{43c}$$

$$\theta_w(\bar{x},\Omega)=\tan^{-1}\frac{\sum_{n=0}^{N}W_n(\bar{x})\bar{q}_{n2}}{\sum_{n=0}^{N}W_n(\bar{x})\bar{q}_{n1}}, \tag{44a}$$

$$\theta_{wc}(\bar{x}_c,\Omega)=\tan^{-1}\frac{\sum_{n=0}^{N}W_n(\bar{x}_c)\bar{q}_{n2}}{\sum_{n=0}^{N}W_n(\bar{x}_c)\bar{q}_{n1}}, \tag{44b}$$

$$\theta_z(\Omega)=\phi-\theta_{fc}. \tag{44c}$$

Physically, Δ_z and Δ_{wc} provide information describing the vibration transmission from the exciting wave system to the ship and equipment, because the wave height a is chosen as a characteristic length in the nondimensional equations.

6. Power flow analysis

Once the nonlinear dynamic displacement variables are solved, the associated vibratory power flow is calculated from the inner product of the force and the corresponding velocity response [14].

6.1. Input power flow

The instantaneous input power flow density p_{in} at any point $\bar{x}$ by a wave is defined by the dot product of the velocity $\dot{\bar{w}}(\bar{x},\Omega,T)$ and fluid loading $\bar{f}_{\xi}(\bar{x},\Omega,T)$. That is

$$p_{\text{in}}=\bar{f}_{\xi}(\bar{x},\Omega,T)\cdot\dot{\bar{w}}(\bar{x},\Omega,T),\quad \bar{x}\in[0,\bar{L}], \tag{45}$$

where

$$\bar{f}_{\xi}(\bar{x},\Omega,T)=(\bar{k}_w-\bar{\rho}_a\Omega^2)\sin(\bar{k}\bar{x}-\Omega T)-\bar{b}\Omega\cos(\bar{k}\bar{x}-\Omega T) \tag{46a}$$

and

$$\dot{\bar{w}}(\bar{x},\Omega,T)=-\Omega\Delta_w(\bar{x},\Omega)\sin(\Omega T-\theta_w) \tag{46b}$$

is the velocity response at any point on the beam. The time-averaged power flow spectrum $\langle p_{\text{in}}\rangle$ is defined by

$$\langle p_{\text{in}}\rangle=\frac{1}{\bar{T}}\int_0^{\bar{T}}\bar{f}_{\xi}(\bar{x},\Omega,T)\cdot\dot{\bar{w}}(\bar{x},\Omega,T)\,\mathrm{d}T, \tag{47}$$

where $\bar{T} = 2\pi/\Omega$. The total instantaneous input power spectrum $P_{\text{in}}(\Omega)$ and its total time-averaged power flow spectrum $\langle P_{\text{in}}(\Omega)\rangle$ are respectively calculated by the integral of p_{in} and $\langle p_{\text{in}}\rangle$ along the length of the beam. That is,

$$P_{\text{in}}(\Omega) = \int_0^{\bar{L}} p_{\text{in}}\, \mathrm{d}\bar{x}, \tag{48}$$

$$\langle P_{\text{in}}(\Omega)\rangle = \int_0^{\bar{L}} \langle p_{\text{in}}\rangle\, \mathrm{d}\bar{x}. \tag{49}$$

6.2. Power flow transmission

To characterize vibratory energy transmission from wave to the equipment, the instantaneous power P_e and the time-averaged power $\langle P_e\rangle$ transmitted through the mounting to the equipment are calculated by

$$P_e(\Omega) = \bar{f}_c(\Delta, \dot{\Delta}) \cdot \dot{\bar{z}}(T, \Omega), \tag{50}$$

$$\langle P_e(\Omega)\rangle = \frac{1}{\bar{T}} \int_0^{\bar{T}} P_e\, \mathrm{d}T. \tag{51}$$

It follows from Eqs. (16), (17d), (18), (42), (43c) and (44c) that

$$\bar{f}_c(\Delta, \dot{\Delta}) = R(\Omega)\cos(\Omega T + \phi - \theta_{fc}) = R(\Omega)\cos(\Omega T + \theta_z), \tag{52a}$$

$$\dot{\bar{z}}(T, \Omega) = -\Omega \Delta_z(\Omega)\sin(\Omega T + \theta_z). \tag{52b}$$

The integration of Eq. (51) gives the time-averaged power

$$\langle P_e(\Omega)\rangle = 0. \tag{52c}$$

This is the first-order approximation result using the harmonic balance method. It shows that the nonlinear system is now represented by an equivalent linear system whose parameters are frequency dependent. For a prescribed nonlinear system and wave frequency ω_e, the nondimensional frequency Ω is constant and therefore the parameters of the equivalent linear system are determined. As demonstrated for linear systems in Ref. [44], the time-averaged changes of the kinetic and potential energy vanish and the time-averaged energy input into a subsystem equals to the time-averaged energy dissipation within this subsystem. Here, the equipment is treated as a rigid body having no internal material damping and therefore, at frequency Ω the time-averaged energy input into the equipment is zero.

The nondimensional instantaneous kinetic energy per unit mass of the equipment is given by

$$e_k(T, \Omega) = \tfrac{1}{2}\dot{\bar{z}}^2(T, \Omega) = E_k(\Omega)\sin^2(\Omega T + \theta_z), \tag{53a}$$

where

$$E_k(\Omega) = \frac{1}{2}\Omega^2 \Delta_z^2(\Omega) = \frac{R^2(\Omega)}{2\Omega^2} \tag{53b}$$

denotes the amplitude of the kinetic energy at each nondimensional frequency $\Omega = \omega_e/\Omega_0$. This quantity is used to estimate the vibration energy spectra of the rigid equipment excited by external wave excitations.

6.3. Power flow absorption

Power flow absorption quantities are used to investigate power flow control effectiveness. The aim of power flow control is to absorb vibratory energy or to minimize its transmission to vibration-sensitive equipment through an isolation system. By using the power flow generation and transmission equations described previously, the instantaneous and time-averaged power flow absorbed by the nonlinear isolator can be derived. That is, the instantaneous power flow P_a and the time-averaged power flow $\langle P_a \rangle$ absorbed by the nonlinear isolator are given, respectively, by

$$P_a = \dot{\Delta} \cdot \bar{f}_c(\Delta, \dot{\Delta}), \tag{54}$$

$$\langle P_a(\Omega) \rangle = \frac{1}{\bar{T}} \int_0^{\bar{T}} P_a \, \mathrm{d}T, \tag{55}$$

where, from Eq. (14)

$$\dot{\Delta} = -\Omega \Delta_1 \sin(\Omega T + \phi). \tag{56}$$

From Eqs. (16), (18), (55) and (56) it follows after integration that

$$\langle P_a(\Omega) \rangle = \eta \lambda_p (\Delta_1 \Omega)^{p+1} \tag{57}$$

describes the time-averaged power absorption $\langle P_a \rangle$.

7. Numerical results and discussions

Numerical simulations of the interactive nonlinear isolation system as illustrated in Fig. 1 were undertaken to investigate its dynamical behaviour, power flow characteristics and isolation efficiency. The system parameters are described as follows: the beamlike ship's principal dimensions are $L = 1.43 \times 10^2$ m (waterline), $B = 21.3$ m, $d = 7.50$ m with a displacement $M_b = 2.35 \times 10^7$ kg, $EI = 5.43 \times 10^{12}$ N m^2; the equipment: $M = 9.60 \times 10^3$ kg; isolator: $K = 1.92 \times 10^6$ N m^{-1}, $C = 2.00 \times 10^3$ Ns m^{-1}, mounting position: $x_c = L/4$. Values of the nonlinear indices examined in this investigation are:

(1) Nonlinear damping only ($q = 1$):
   (i) $p < 1$: $p = 0.5$; (ii) $p > 1$: $p = 1.5$, $p = 2$ (quadratic damping model), $p = 3$;
(2) Nonlinear stiffness only ($p = 1$):
   (i) $q < 1$: $q = 0.5$; (ii) $q > 1$: $q = 2$;
(3) Combination of cases (1) and (2).

Sinusoidal waves of wavelength $\lambda = 15$, 50 m, $2L$, L, $L/2$, $0.35L$, $L/4$ with wave amplitude $a = 1$ m were examined to explore the effect of wavelength. To investigate the effects of elastic supporting structure, the two rigid body heave and pitch modes and the first three elastic modes of

the beam were assumed to cover the wave frequency bandwidth of interest [39]. The time-averaged input power and the kinetic energy of the equipment for different nonlinear isolator models were calculated in the frequency domain. The power flow spectra are expressed in decibel scale (dB reference: 10^{-12} w). These results are compared with the linear case $p = 1 = q$.

7.1. Input power spectra

7.1.1. Effect of elastic supporting structure

Figs. 2 and 3 illustrate the effect of the flexible ship model, compared with a rigid ship model, on the time-averaged input power flow spectrum $\langle P_{\text{in}} \rangle$ of the linear system excited by a sinusoidal wave of wavelength $\lambda = 50$ or 15 m. The results reveal that the isolation system mounted on the elastic ship travelling in sinusoidal waves has a more complex dynamical behaviour than for the rigid ship case due to the dynamical characteristics of the compliant ship structure. As shown in these two figures, there are five peaks at the frequency ratios $\Omega = 0.08$, 0.08, 0.45, 1.22, 2.39 on the curve of time-averaged input power flow spectrum. These peaks correspond to the two rigid modes at frequency 0.18 Hz (repeat frequency) and three elastic modes at frequencies 1.01, 2.75 and 5.37 Hz, respectively. This evidence indicates the importance of considering the elastic effects of the ship in designing an effective isolation system.

As shown in Fig. 2, the input power flow value produced by the ship's elastic modes is about 20 dB higher than the rigid ship model under the wave excitation of wavelength 50 m. This difference reduces to 8 dB when the excitation is of wavelength 15 m shown in Fig. 3. From this

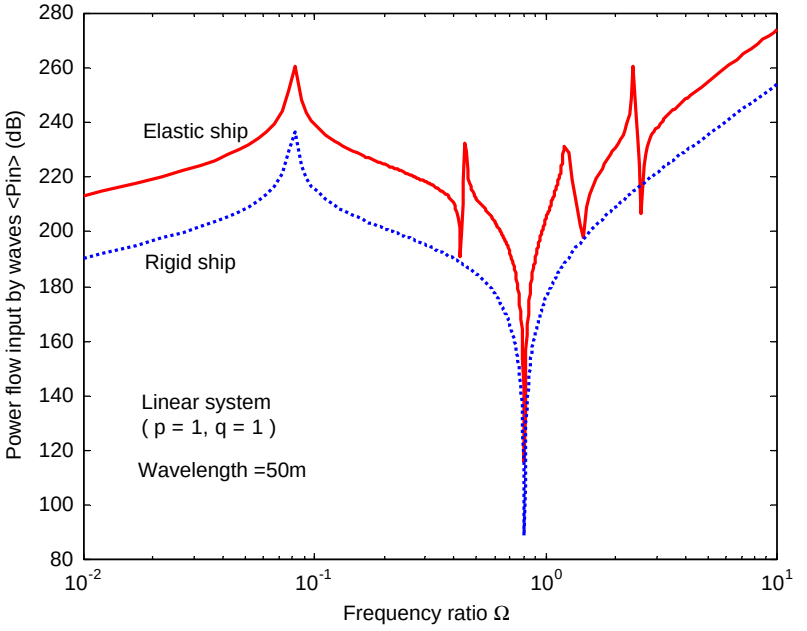

Fig. 2. Power input by wave of wavelength 50 m for different system models (····· rigid base model; ——, elastic beam-like ship model).

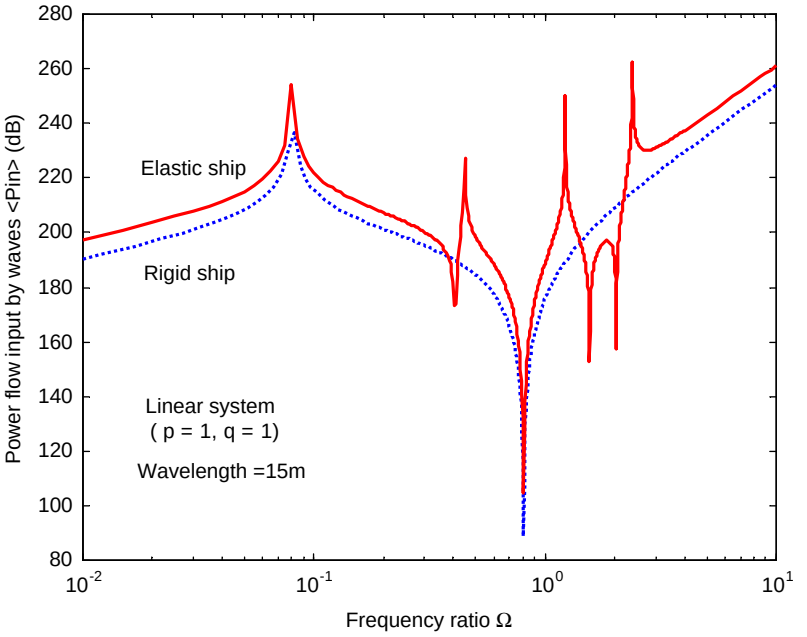

Fig. 3. Power input by wave of wavelength 15 m for different system models (key: as Fig. 2).

comparison, it may be concluded that the simplified rigid model underestimates the input vibratory energy of the sea. Therefore, for a safe design the elastic dynamic characteristics of the supporting structure needs to be considered. However, from a vibration control viewpoint, this evidence suggests that increasing hull stiffness and therefore its elastic natural frequency is beneficial in reducing vibration transmission from the base to the equipment.

7.1.2. Effect of sea wave length

To examine the effect of wave condition, five different sinusoidal waves of wavelength $\lambda = 2L$, L, $L/2$, $0.35L$ and $L/4$ were examined for the linear system accepting the ship as an elastic beam. Figs. 4 and 5 display, respectively, the variations of the total time-averaged input power spectra of these sinusoidal wave excitations in the linear and nonlinear coupled systems. The results presented in Fig. 4 reveal that the wave excitation has significant influence on power flow input to the overall system. This is because the ship travelling in waves changes its location along the wave, and, hence, varies the phase magnitude between ship motion and fluid load. Also, changing wavelength alters the wave force distributions along the ship and, hence, modifies the amplitude of generalised force, as shown in Eq. (9), for each mode. As observed in Fig. 4, for $\lambda = 2L$ the power input by the wave is the largest because the wave-induced pressures and inertia forces along the ship are in phase with the vertical motion of the beam-like ship and the wave distribution corresponds to the greatest generalized force. When ship-wave matching occurs [39], i.e., $\lambda = L$, the energy input into heave, pitch and elastic bending modes is greater than those predicted for shorter wavelengths ($\lambda < L$). For example, for wavelength $\lambda = L/4$ the input power by the wave is about 30 dB less compared to the case of wavelength $\lambda = L$, as observed from Fig. 4. Further

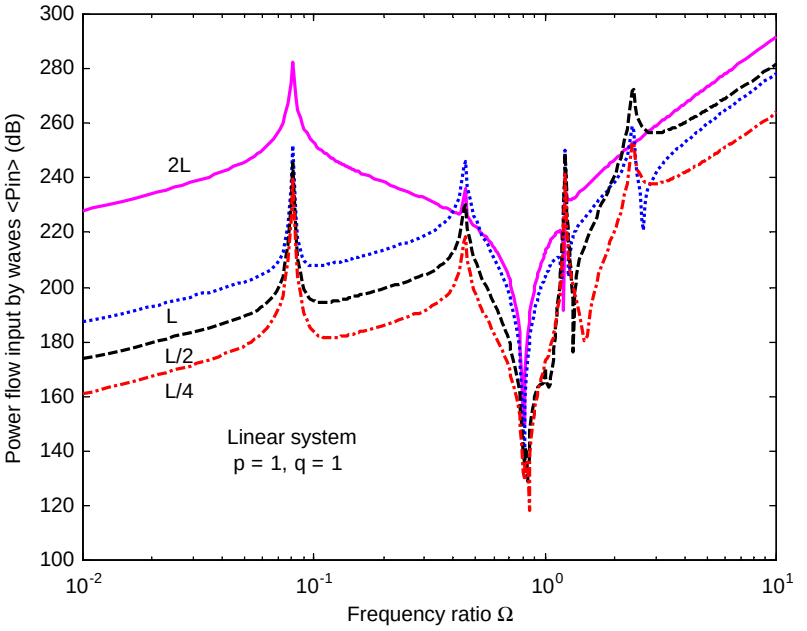

Fig. 4. Influence of wavelength on the time-averaged power input of the linear interactive system ($p = 1$, $q = 1$).(——, $\lambda = 2L$; · · · · · ·,$\lambda = L$; – – –, $\lambda = L/2$; – — – — –, $\lambda = L/4$).

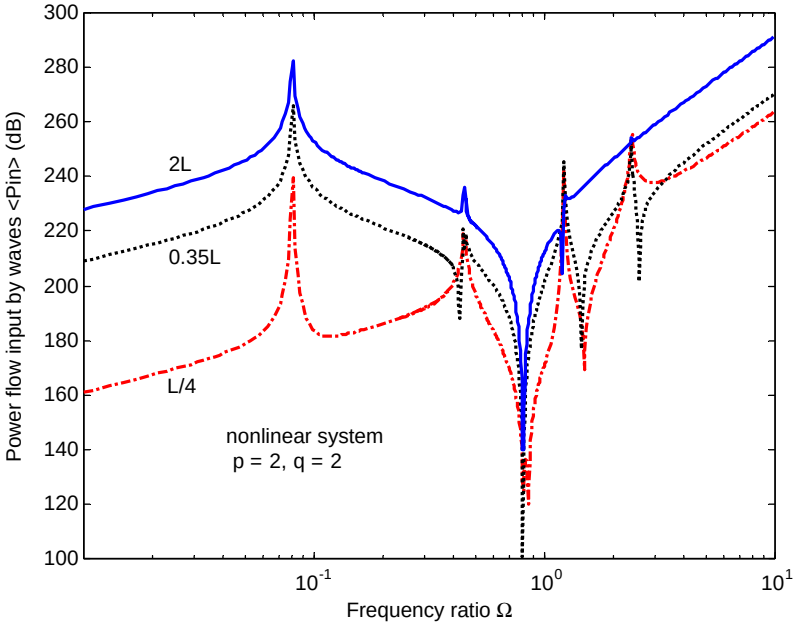

Fig. 5. Influence of wavelength on the time-averaged power input of the nonlinear interactive system ($p = 2$, $q = 2$). (——, $\lambda = 2L$; · · · · · ·, $\lambda = 0.35L$; – — – — –, $\lambda = L/4$).

numerical simulations demonstrated that the power flow input by the waves reduces as the wavelength decreases. For the nonlinear case, Fig. 5 shows the influence of wavelengths on the input power spectra. This exhibits similar trends over the full frequency range as observed in the linear case in Fig. 4.

7.1.3. *Effect of nonlinear damping*

To examine the effect of nonlinear damping alone, four different values of the damping exponent $p = 0.5$, 1, 2 and 3 were considered assuming a constant value of stiffness exponent $q = 1$. Figs. 6 and 7 illustrate their influence on the time-averaged input power. In these figures, the solid lines represent the linear system, whereas other lines relate to the nonlinear cases as indicated in the figures.

Several observations are deduced from the findings displayed in these figures. Namely, (1) the nonlinearity in the damper alters the input power flow characteristics locally. As shown in Fig. 6(a), there is no obvious global effect of the damping power p on the time-averaged input power spectra in the chosen frequency range, but a local effect is observed as highlighted in details in Fig. 6(b) and Fig. 7(a,b). (2) This local difference of the peak values of the input power increases as p increases (see Figs. 6(b) and 7). (3) The peak values of the input power are always larger for $p > 1$ than the linear case ($p = 1$). (4) Similar trends are also observed for other types of wave excitation of different wavelengths ($\lambda = L/2, L/4$) as shown in Fig. 7(a,b), and the input power increases as the nonlinear exponent p increases. This is because an increase of the damping power p increases the equivalent damping coefficient η given in Eq. (12). Fig. 8 clearly supports this trend. This explains why increasing p results in an increased power flow input, because the dissipative capacity of the system is increased.

7.1.4. *Effect of nonlinear stiffness*

The nonlinear stiffness influence on the time-averaged input power $\langle P_{\text{in}} \rangle$ is examined by setting the damping power $p = 1$ and varying the stiffness power $q = 0.5$, 1, 2, as shown in

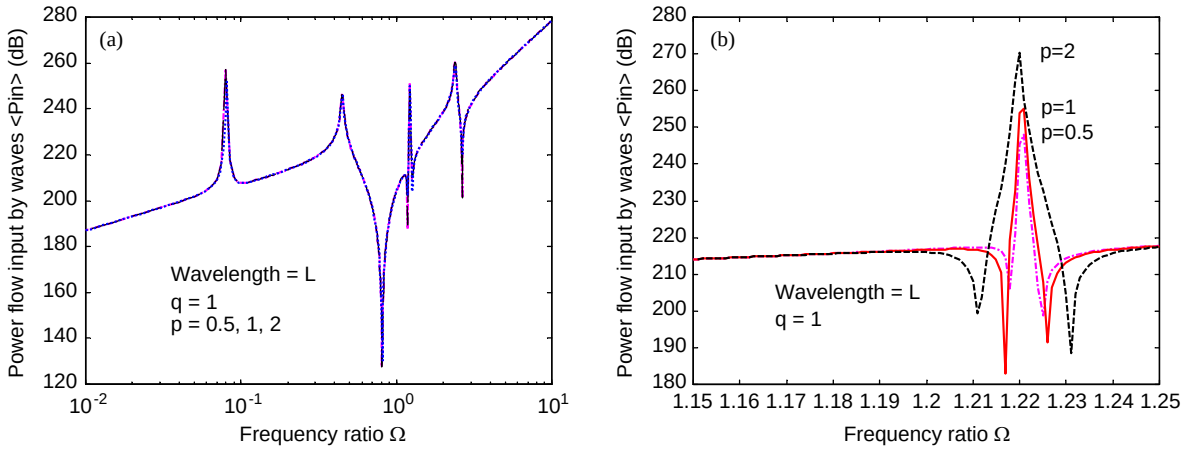

Fig. 6. Effect of nonlinear damping on the time-averaged power flow input to the system ($q = 1$, $\lambda = L$): (a) overall effect, (b) local effect. (– — – — –, $p = 0.5$; ——, $p = 1$; – — – — –, $p = 2$).

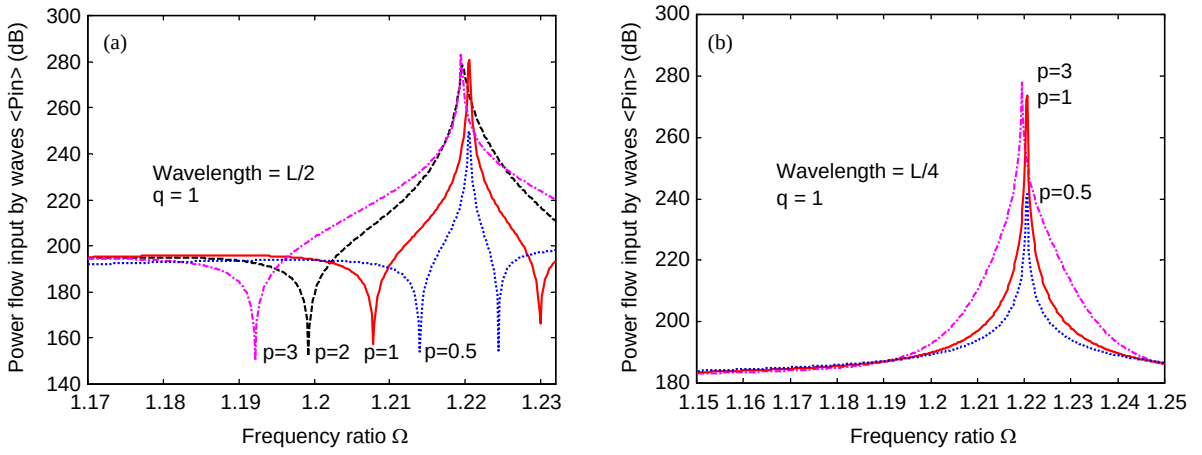

Fig. 7. Local effect of nonlinear damping on the time-averaged power flow input to the system ($q = 1$): (a) $\lambda = L/2$, (b) $\lambda = L/4$. (·····, $p = 0.5$; ——, $p = 1$; – – –, $p = 2$; – — – — –, $p = 3$) .

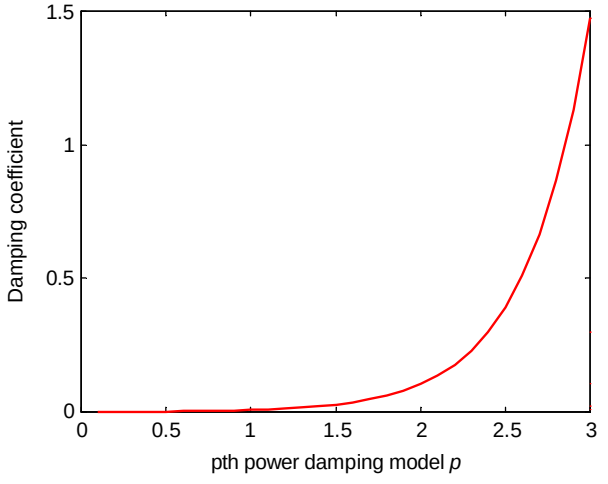

Fig. 8. Variation of the damping coefficient η to the nonlinear damping power p ($\eta = Ca^{p-1}\Omega_0^{p-2}/2M$, wave height $a = 1$ m).

Fig. 9(a,b). Again, the solid line in these figures represents the linear case ($p = 1$, $q = 1$), whereas the dotted and dashed lines denote the nonlinear cases.

It is seen from Fig. 9(a) that the input power spectra corresponding to the first two and fourth peaks are almost unaffected by the nonlinearity of the isolator stiffness. However, there is considerable reduction of the input power at the third peak which corresponds to the resonance frequency at $\Omega = 1.22$ of the coupled system. This local effect is highlighted in Fig. 9(b) in the region of $\Omega = 1.22$.

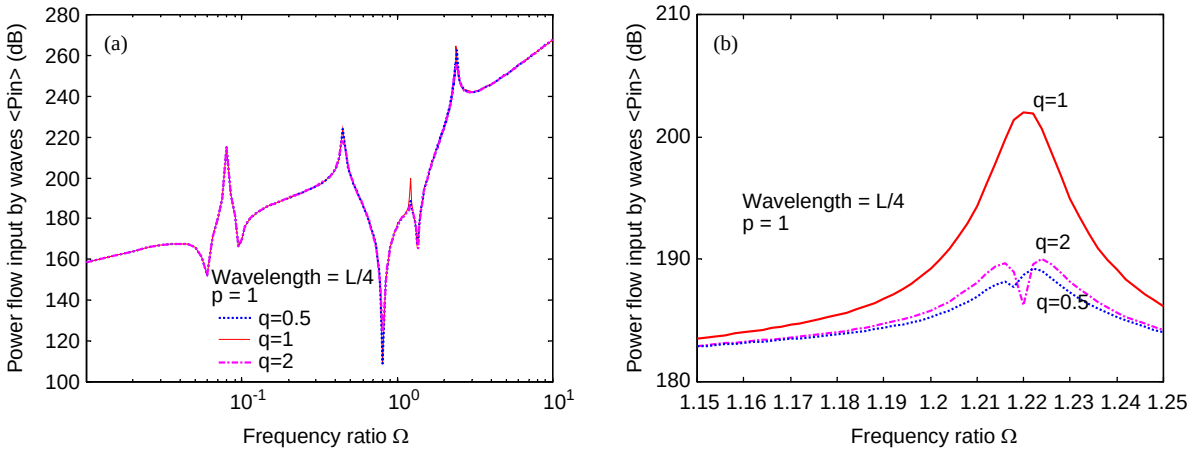

Fig. 9. Effect of nonlinear stiffness on power flow input ($\lambda = L/4$, $p = 1$): (a) global effect, (b) local effect. (· · · · · ·, $q = 0.5$; ——, $q = 1$; – — – — –, $q = 2$).

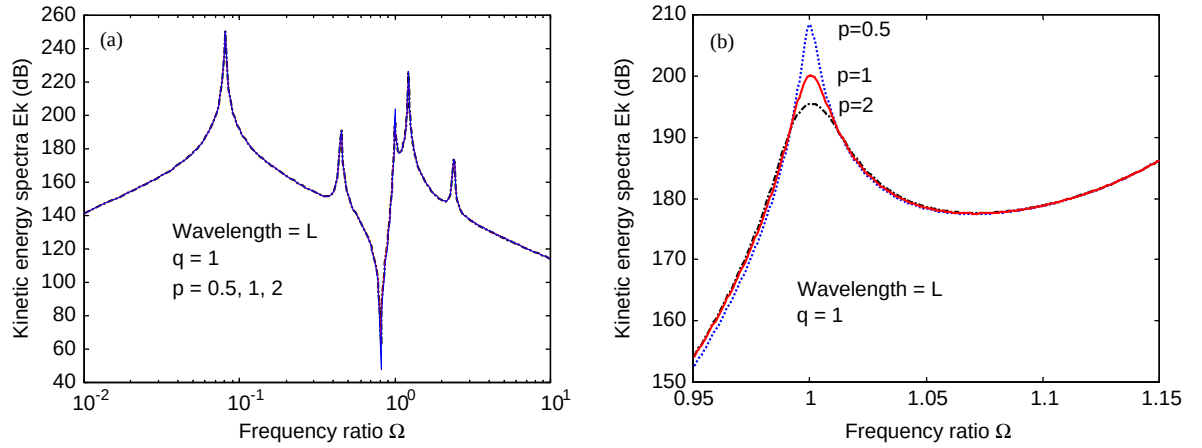

Fig. 10. Effect of nonlinear damping on the kinetic energy of equipment ($\lambda = L$, $q = 1$): (a) global effect, (b) local effect. (· · · · · ·, $p = 0.5$; ——, $p = 1$; – — – — –, $p = 2$).

7.2. Kinetic energy spectra of the equipment

7.2.1. Effect of nonlinear damping

The effectiveness of the nonlinear vibration isolation system is now examined through the kinetic energy spectra E_k associated with the equipment. Fig. 10 compares the kinetic energy spectra for different damping models (i.e., $p = 0.5,1,2$) with linear stiffness ($q = 1$) when the elastic ship is subject to wave excitation $\lambda = L$. It is observed from Fig. 10(a) that the damping power p has no obvious influence on the global kinetic energy spectra E_k. However, it is noted that the damping effect significantly influences the kinetic energy spectra at the resonance

frequency of the mounting system (i.e., $\Omega = 1$) as highlighted in Fig. 10(b). Compared to the linear results, the kinetic energy spectrum decreases in value for $p > 1$ implying power dissipation in the nonlinear mount is achieved for strong nonlinearity in damping ($p > 1$). For $p < 1$, an increase in the value of the kinetic energy spectrum occurs. Further calculations show that a decrease of power p increases the kinetic energy spectrum and an increase in power p reduces the peak value of the vibration energy experienced by the equipment. Moreover, this tendency is also observed for a system with nonlinear damping but linear stiffness ($q = 1$) under other forms of sinusoidal wave excitation. This demonstrates that for $p > 1$ nonlinear damping is effective in reducing the power transmission from ship hull to equipment. When nonlinearity is also present in the stiffness ($q \neq 1$) of the isolator, it is shown in Figs. 13 and 14 that the kinetic energy spectra are also dramatically affected globally in the high-frequency region by damping characteristic.

7.2.2. *Effect of nonlinear stiffness*

The effect of nonlinear stiffness with linear damping ($p = 1$) on the kinetic energy spectra E_k of the equipment mounted on a rigid base structure is initially examined. Since the nonlinearity of stiffness causes discontinuous jumps in the frequency sweep process, increasing and decreasing frequency sweep processes were performed in the numerical simulation of the Newton–Raphson iterative method in order to characterize the kinetic energy spectra over the full frequency range considered. Fig. 11 shows the influence of hardening ($q = 2$) and softening ($q = 0.5$) stiffness nonlinearities on E_k in comparison with the linear case. It is seen that a jump phenomenon occurs in the curves for both $q = 0.5$ and 2 in the respective critical frequency ranges. Therefore, an

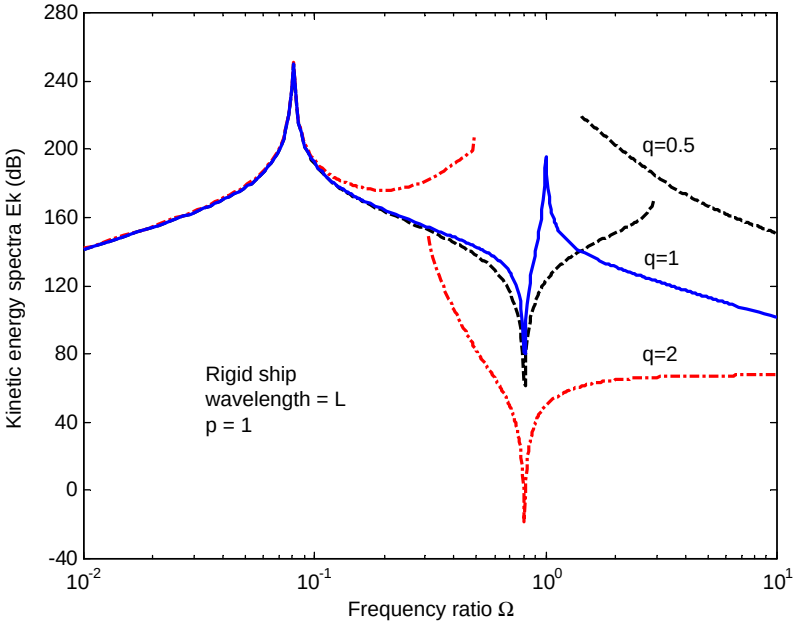

Fig. 11. Effect of nonlinear stiffness ($q = 0.5$, 2) on the kinetic energy of equipment compared to linear case for rigid ship model ($\lambda = L$, $p = 1$).

unstable solution of the system's governing equations exists in the frequency range within the jump bandwidth. It is interesting to note that for $q = 0.5$ a reduction in the energy spectrum occurs before the critical frequency Ω_c and thereafter an increase compared to a linear stiffness system. In contrast, for $q = 2$ the energy spectrum exhibits the opposite behaviour. That is, a large reduction occurs after the corresponding critical frequency Ω_c, whereas in the low-frequency region, the nonlinear stiffness only negligibly affects the energy spectra corresponding to the rigid modes of the beam.

Treating the ship as a flexible beam-like structure, we examine the effect of nonlinearity in the isolator's stiffness. Fig. 12 illustrates the kinetic energy spectra E_k for a system with softening ($q = 0.5$) and hardening ($q = 2$) stiffnesses assuming linear damping ($p = 1$). These results are compared to the linear model ($p = 1 = q$) predictions indicated by the solid line in the figure. Fig. 12 reveals a similar dynamical behaviour in the low-frequency region as shown in Fig 11. Breaks in the solution paths also exist and are similar in form to the ones discussed in Fig. 11. However, no strong jump phenomena are predicted in each critical frequency range. It is also seen that the critical frequency ranges covering the discontinuity in Fig. 12 are narrower and less evident than observed in Fig. 11, which reflect the role played by material damping in the flexible ship model. Further numerical simulations confirm this finding, implying that an increasing loss factor associated with the ship structure prohibits the existence of a discontinuity.

7.2.3. *Nonlinear stiffness and nonlinear damping influences*

We now examine the effect of nonlinearities in both damping and stiffness properties of the isolator system. The impact of this nonlinear configuration on energy spectra behaviour

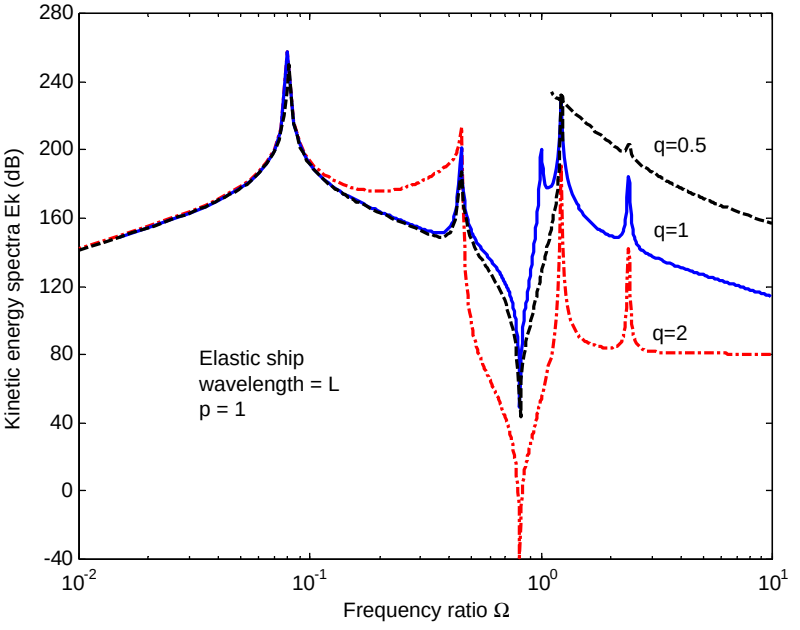

Fig. 12. Effect of nonlinear stiffness ($q = 0.5, 2$) on the kinetic energy of equipment compared to linear case for elastic ship model ($\lambda = L$, $p = 1$).

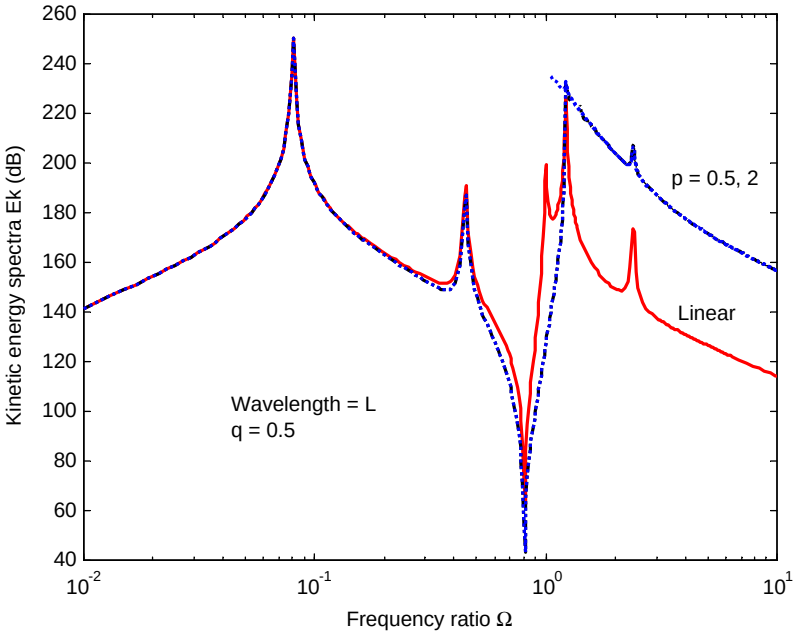

Fig. 13. Effect of softening nonlinear stiffness ($q = 0.5$) and nonlinear damping ($p = 0.5$, 2) on the kinetic energy of equipment for elastic ship model ($\lambda = L$).

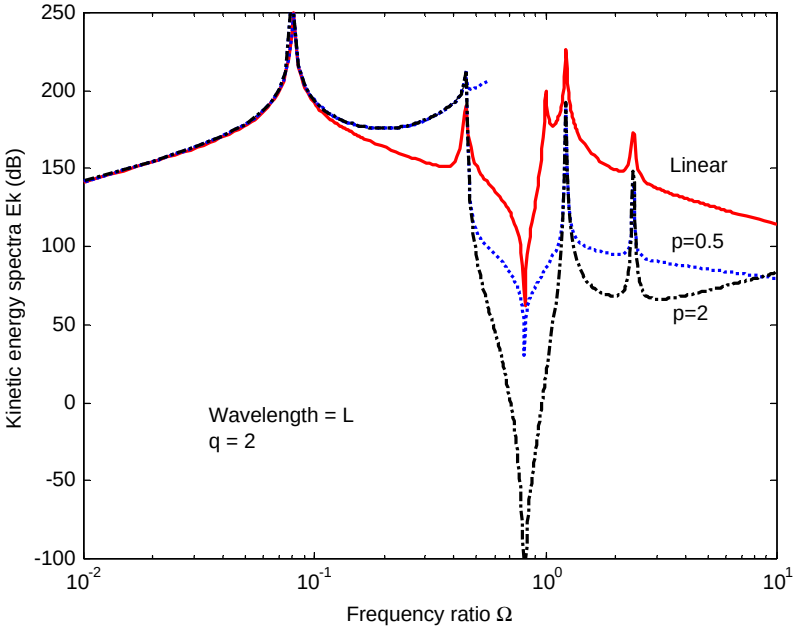

Fig. 14. Effect of hardening nonlinear stiffness ($q = 2$) and nonlinear damping ($p = 0.5$, 2) on the kinetic energy of equipment for elastic ship model ($\lambda = L$).

of the equipment is assessed by comparing predictions to the linear case ($p = 1 = q$). The energy spectra for the system with softening ($q = 0.5$) and hardening ($q = 2$) stiffnesses for different nonlinear damping indices ($p = 0.5,\ 2$) are presented in Figs. 13 and 14, respectively. Results for $p = 1,\ q = 0.5$ and 2 were discussed in Section 7.2.2 and these are compared to the linear model ($p = 1 = q$) predictions indicated by the solid line in both figures.

In both nonlinear stiffness cases, Figs. 13 and 14 illustrate a jump phenomenon near the respective critical frequency regimes indicating multiple solutions and hence difficulties in representing spectra curve solutions. In addition, the jump occurs at a much lower-frequency region for the system with strong stiffness ($q > 1$) nonlinearity in comparison with results derived for the softening ($q < 1$) nonlinearity case. A comparison of Fig. 14 with Fig. 13 in the high-frequency region shows the positive benefit of a hardening stiffness associated with nonlinear damping on the kinetic energy spectra. That is, after the critical frequency the level of energy transmission is much lower in a system with a strong stiffness nonlinearity (Fig. 14) than one with a weak stiffness nonlinearity (Fig. 13). In the low-frequency region ($\Omega < 0.08$, corresponding to rigid ship motions), in both cases the effect of nonlinear damping is similar to the linear stiffness ($q = 1$) case. Moreover, for $q > 1$ the kinetic energy reduction increases as the strength of the damping nonlinearity increases as shown Fig. 14. This implies that using a nonlinear damper in conjunction with a strong stiffness characteristic is beneficial for vibration reduction in the system. For $q < 1$, an increase in the value of damping power p has no beneficial decrease in the equipment's kinetic energy.

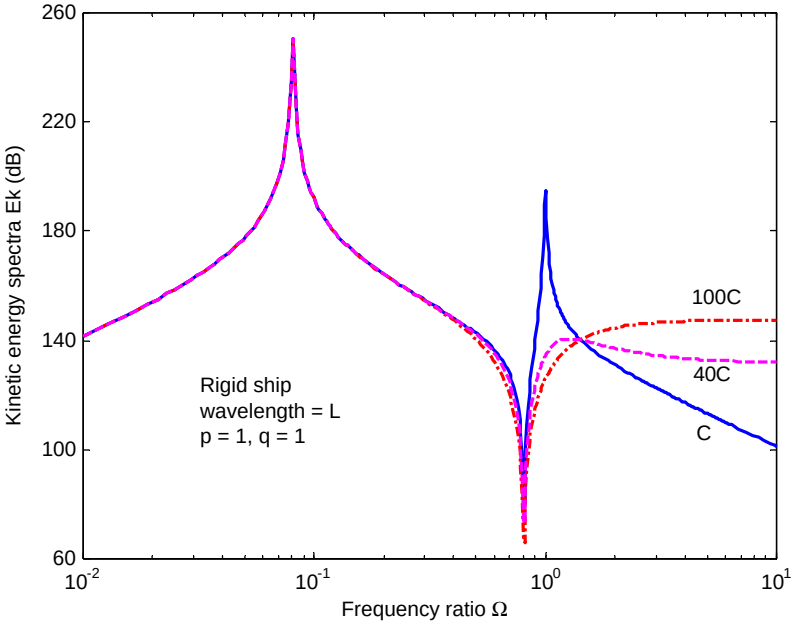

Fig. 15. Effect of damping coefficient C on the kinetic energy of equipment in linear interactive system ($\lambda = L, p = 1, q = 1$).

7.2.4. Influence of passive damping in linear and nonlinear system

In the linear isolation system, increasing damping coefficient C yields an increased power transmission when $\Omega > 1.414$ as displayed in Fig. 15 for the rigid ship model. This implies that the heavily damped linear vibration isolator produces poor vibration isolation in the high-frequency region, which coincides with traditional vibration isolation theory [1–4]. However, in a nonlinear system, increasing the damping coefficient C may have a positive effect in certain frequency ranges.

Fig. 16 illustrates the influence of varying the value of the damping coefficient C on the kinetic energy spectra E_k with nonlinearities in both stiffness and damping ($p = 2$, $q = 2$). It is observed that the discontinuities in the curve E_k caused by nonlinear stiffness ($q = 2$) as shown in Fig. 16 (indicated by the solid line) and previously in Figs. 11 and 14 (indicated by the dash-dotted line) are absent when the damping coefficient C is increased by a factor of 40 times the original value. Results presented in Fig. 16 show that further increasing the value C (i.e., $100C$) smoothes the curve near the critical frequency and a large energy transmission occurs after the critical frequency.

In general, when nonlinearities exist in damping and stiffness, the damping parameter C significantly influences the characteristics of the kinetic energy spectra. The jump phenomenon is noticeable in predictions of E_k for small damping coefficient value C. Increasing C smoothes the spectra curve and stabilises the nonlinear system. On the other hand, when the nonlinearity is present in damping only (see Fig. 10), no jump effect is exhibited in the energy spectra even for a small value of damping coefficient.

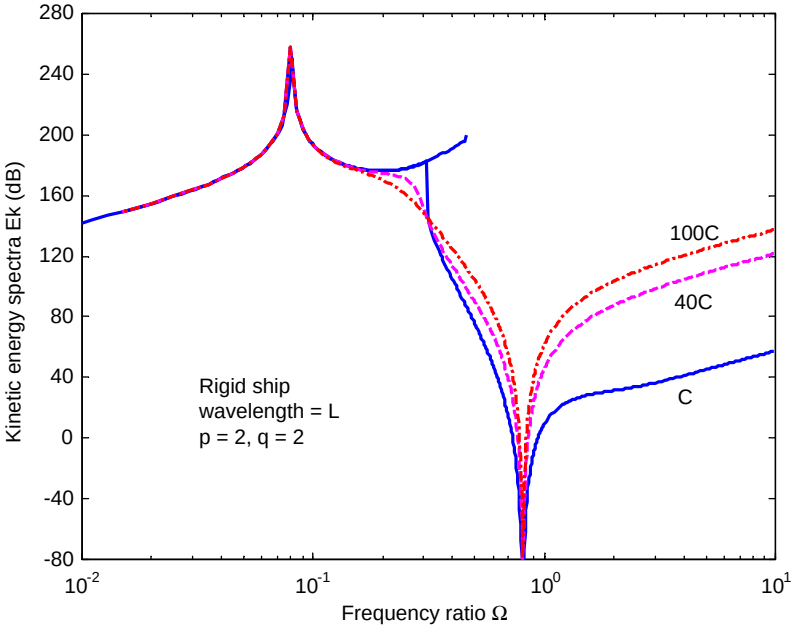

Fig. 16. Effect of damping coefficient C on the kinetic energy of equipment in nonlinear interactive system ($\lambda = L$, $p = 2$, $q = 2$).

In general, Figs. 13–16 demonstrate that using an isolator characterized by strong nonlinear damping ($p>1$) and hardening stiffness ($q>1$) as well as a large passive damping coefficient C produces substantial reductions of the energy transmitted to the equipment.

7.3. Comment

Jump phenomena cause difficulty in defining the exact form of the power flow spectra curves because of the nonuniqueness of solution in the vicinity of the jump frequency band. This may be overcome by developing an arc-length method [45] in the frequency domain so as to characterize power transmission behaviour within the critical frequency band. This requires further investigation which could lead to the characterization of bifurcation and chaos from an energy flow viewpoint allowing extension of the synthesis method to encompass a multi-term harmonic balance method.

8. Conclusions

This study discusses mechanisms underlying understanding of power flow characteristics in a complex nonlinear system influenced by the dynamics of a compliant support (i.e., ship hull) excited by a distributive dynamical loading due to sinusoidal waves. The nonlinear system comprises of components such as equipment (e.g. machinery), isolator, flexible ship and waves with the isolator characterized by nonlinear properties in both the damping and stiffness. This nonlinear interactive system excited by waves is examined from a vibratory power flow perspective.

The nonlinearity of the isolator is described by a pth power model for damping and qth power for stiffness. A mathematical model describing the dynamics of the nonlinear interactive system is developed and governing equations are formulated to examine dynamical interaction behaviour and power flow characteristics. A harmonic balance method in association with a Newton–Raphson iteration process and an efficient numerical algorithm are developed to solve the equations of this nonlinear dynamical system. Numerical simulations of the system are undertaken and the dynamical behaviour, power flow characteristics and isolation efficiency of the complex nonlinear equipment–beam–water isolation system investigated. The power flow input produced by waves to the system and the vibratory energy experienced by the equipment are examined for different nonlinear configurations and different wave excitations. The influence of flexible or rigid ship, the effects of nonlinearities in damping or/and in stiffness, and the impact of different wave excitations on power flow characteristics are studied. The primary findings of this investigation are as follows.

(1) The input power flow spectrum is not globally sensitive to the nonlinearity in damping and stiffness of the isolator except for local variations at some resonance frequency of the coupled system.
(2) The nonlinearity in stiffness plays an important role in determining the characteristics of power transmission. At critical frequencies, a jump phenomenon is observed in predicted power transmission values especially in the vicinity of the first few natural frequencies of the

system where peak power occurs. Therefore, nonuniqueness and instability in the power transmission path exist in the frequency range containing the jump phenomenon. The existence of multiple power flow transmission paths for the same excitation is one of the main differences observed between nonlinear and linear systems.

(3) Power flow characteristics, before and after the critical frequency Ω_c, have different behaviours. When $\Omega < \Omega_c$, the kinetic energy transmitted to the equipment reduces as the value of q reduces but increases as q reduces for $\Omega > \Omega_c$.

(4) The contribution of nonlinear damping is significant at the isolator's resonance frequency in reducing the peak kinetic energy value of the equipment as p increases.

(5) A nonlinear isolator with hardening stiffness but large damping index value p may prevent jump occurring or the nonlinear system becoming unstable.

The importance of incorporating the dynamic characteristics of the flexible ship structure rather than simplifying the structure as a rigid hull is demonstrated through predictions of the power flow behaviour and through evaluation of isolator effectiveness in the nonlinear interactive system. The findings provide an insight, not only into the dynamical interactive behaviour of equipment/machinery—nonlinear isolator—ship—waves coupled system from an energy transmission perspective, but may be generalized to vibration isolation systems designed or mounted in flexible ships travelling in a seaway. This study provides a theoretical approach to analyse power flow transmissions in a nonlinear system and to produce practical guidelines for the design of a vibration isolation system applicable to maritime engineering. Based on this study, the following design guidelines are drawn:

(1) A ship deck/hull built as rigid as possible is beneficial in reducing vibration transmission from the hull structure to the equipment.

(2) The utilization of a softening nonlinear stiffness ($q < 1$) in the low-frequency range $\Omega < \Omega_c$ and a hardening nonlinear stiffness ($q > 1$) in the high-frequency $\Omega > \Omega_c$ produces benefits in controlling vibration transmission.

(3) An increase of the nonlinear damping power p provides substantial reductions in the power transmission to the equipment at the resonance frequency of the isolator.

References

[1] C.E. Crede, *Vibration and Shock Isolation*, Wiley, New York, 1951.
[2] C.M. Harris, C.E. Crede, *Shock and Vibration Handbook*, McGraw-Hill, New York, 1961.
[3] W.T. Thomson, *Theory of Vibration with Applications*, third ed., Prentice-Hall, Englewood Cliffs, NJ, 1988.
[4] R.E.D. Bishop, D.C. Johnson, *The Mechanics of Vibration*, Cambridge University Press, Cambridge, 1960.
[5] J.S. Tao, G.R. Liu, K.Y. Lam, Design optimization of marine engine-mount system, *Journal of Sound and Vibration* 235 (2000) 477–494.
[6] G. Kim, R. Singh, Non-linear analysis of automotive hydraulic engine mount, *Transactions of the ASME, Journal of Dynamics System, Measurement and Control* 115 (1993) 482–487.
[7] G. Kim, R. Singh, A study of passive and adaptive hydraulic engine mount systems with emphasis on non-linear characteristics, *Journal of Sound and Vibration* 179 (1995) 427–453.
[8] G. Popov, S. Sankar, Modelling and analysis of non-linear orifice type damping in vibration isolator, *Journal of Sound and Vibration* 183 (1995) 751–764.

[9] K. Mallik, V. Kher, M. Puri, H. Hatwal, On the modelling of non-linear elastomeric vibration isolators, *Journal of Sound and Vibration* 219 (1999) 239–253.
[10] J.I. Soliman, M.G. Hallam, Vibration isolation between non-rigid machines and non-rigid foundation, *Journal of Sound and Vibration* 8 (1968) 329–351.
[11] E.E. Ungar, C.W. Dietrich, High-frequency vibration isolation, *Journal of Sound and Vibration* 4 (1966) 224–241.
[12] J.C. Snowden, Vibration isolation: use and characterisation, in: C.L. John (Ed.), *NBS Handbook*, McGraw-Hill, New York, 1978.
[13] D. Sciulli, D.J. Inman, Isolation design for a flexible system, *Journal of Sound and Vibration* 216 (1998) 251–267.
[14] H.G.D. Goyder, R.G. White, Vibrational power flow from machines into built-up structures, *Journal of Sound and Vibration* 68 (1980) 59–117.
[15] R.J. Pinnington, R.G. White, Power flow through machine isolators to resonant and non-resonant beam, *Journal of Sound and Vibration* 75 (1981) 179–197.
[16] B. Petersson, J. Plunt, On effective mobilities in the prediction of structure-borne sound sources based on mobility techniques, *Journal of Sound and Vibration* 82 (1982) 251–267.
[17] J.M. Cuschieri, Structural power-flow analysis using a mobility approach of an L-shape plate, *Journal of Sound and Vibration* 87 (1990) 179–197.
[18] J. Pan, J.Q. Pan, C.H. Hansen, Total power flow from a vibrating rigid body to a thin panel through multiple elastic mounts, *Journal of Acoustical Society of America* 92 (1992) 895–907.
[19] Y.P. Xiong, K.J. Song, Power flow in the coupled dynamic system of machinery and building floor, *Chinese Journal of Acoustics* 15 (1996) 73–80.
[20] Y.P. Xiong, J.T. Xing, W.G. Price, Power flow analysis of complex coupled systems by progressive approaches, *Journal of Sound and Vibration* 239 (2001) 275–295.
[21] Y.P. Xiong, J.T. Xing, W.G. Price, Active vibration control of a human body–seat–boat–water dynamic interaction system excited by waves, *Proceedings of the VIII International Conference on Recent Advance of Structure Dynamics, SD2003*, Southampton, July 14–16, 2003, paper No.11 on CD.
[22] B. Ravindra, A.K. Mallik, Performance of non-linear vibration isolators under harmonic excitation, *Journal of Sound and Vibration* 170 (1994) 325–337.
[23] N.C. Shekhar, H. Hatwal, A.K. Mallik, Performance of non-linear isolators and absorbers to shock excitations, *Journal of Sound and Vibration* 227 (1999) 293–307.
[24] S. Natsiavas, P. Tratskas, On vibration isolation of mechanical systems with non-linear foundations, *Journal of Sound and Vibration* 194 (1996) 173–185.
[25] J.Q. Pan, C.H. Hansen, Active control of power flow from a vibrating rigid body to a flexible panel through two active isolators, *Journal of the Acoustical Society of America* 93 (1993) 1947–1953.
[26] M.J. Brennan, S.J. Elliot, R.J. Pinnington, Strategies for the active control of flexible vibration on beam, *Journal of Sound and Vibration* 186 (1995) 657–688.
[27] Y.K. Koh, R.G. White, Analysis and control of vibrational power transmission to machinery supporting structures subjected to a multiple excitation system—Part I: driving point mobility matrix of beam and rectangular plates, *Journal of Sound and Vibration* 196 (1996) 469–493.
[28] Y. Xiong, K. Song, Optimum control of vibration and structure-borne noise for machinery on flexible foundation, *Chinese Journal of Mechanical Engineering* 9 (1996) 13–20.
[29] P. Gardonio, S.J. Elliott, Passive and active isolation of structural vibration transmission between two plates connected by a set of mounts, *Journal of Sound and Vibration* 237 (2000) 483–511.
[30] Y.P. Xiong, J.T. Xing, W.G. Price, Hybrid, active and passive control of vibratory power flow in flexible isolation systems, *Shock and Vibration* 7 (2000) 139–148.
[31] Y.P. Xiong, J.T. Xing, W.G. Price, A general linear mathematical model of power flow analysis and control for integrated structure-control systems, *Journal of Sound and Vibration* 267 (2003) 301–334.
[32] T.J. Royston, R. Singh, Optimization of passive and active non-linear vibration mounting systems based on vibratory power transmission, *Journal of Sound and Vibration* 194 (1996) 295–316.
[33] T.J. Royston, R. Singh, Vibratory power flow through a non-linear path into a resonant receiver, *Journal of Acoustical Society of America* 101 (1997) 2059–2069.

[34] Y.P. Xiong, J.T. Xing, W.G. Price, Power flow analysis of an equipment—non-linear isolator—flexible ship interaction system excited by progressive sea waves, *Proceedings of the Tenth International Congress on Sound and Vibration*, 2003, pp. 4841–4848.
[35] C. Hayashi, *Non-linear Oscillations in Physical Systems*, Princeton University Press, Princeton NJ, 1985.
[36] W.H. Press, B.P. Teukolsky, W.T. Vetterling, *Numerical Recipes: The Art of Scientific Computing*, University Press, Cambridge, 1986.
[37] R.E.D. Bishop, W.G. Price, Y. Wu, A general linear hydroelasticity theory of floating structures moving in a seaway, *Philosophical Transactions of the Royal Society of London Series A* 316 (1986) 375–426.
[38] R.E.D. Bishop, On the strength of large ships in heavy seas, *South African Mechanical Engineer* 21 (1971) 2–17.
[39] R.E.D. Bishop, W.G. Price, *Hydroelasticity of Ships*, University Press, Cambridge, 1979.
[40] S.M. Metwalli, Optimum nonlinear suspension systems, *Transactions of the ASME, Journal of Mechanism, Transmission and Automation in Design* 180 (1986) 197–202.
[41] L. Azrar, R. Benamar, R.G. White, A semi-analytical approach to the non-linear dynamic response problem of beams at large vibration amplitudes—part II—multimode approach to the steady state forced periodic response, *Journal of Sound and Vibration* 255 (2002) 1–41.
[42] M. Abramowitz, I.A. Stegum, *Handbook of Mathematical Functions*, nineth ed, Dover Publications Inc., New York, 1972.
[43] B. Noble, *Applied Linear Algebra*, Prentice-Hall Inc., Englewood Cliffs NJ, 1969.
[44] J.T. Xing, W.G. Price, A power-flow analysis based on continuum dynamics, *Proceedings of the Royal Society of London Series A* 455 (1999) 401–436.
[45] M.A. Crisfield, *Non-linear Finite Element Analysis of Solids and Structures*, Vol. 2, Advanced Topics, Wiley, Chichester, 1997.